공학박사 학위논문

전기이륜차의 도로 부하를 구하는 새로운 방법과 모터 다이나모미터에서 주행 성능을 평가하는 시뮬레이터 개발

New torque-speed balance method to determine road load of electric two-wheeler and development of hardware-in-the-loop simulator for its driving performance testing on motor dynamometer

2016 년 2 월

서울대학교 대학원

기계항공공학부

강 대 경

Abstract

New torque-speed balance method to determine road load of electric two-wheeler and development of hardware-in-the-loop simulator for its driving performance testing on motor dynamometer

Dae Kyung Kang
Department of Mechanical and Aerospace Engineering
The Graduate School
Seoul National University

In this study, the new method to determine road load of electric two-wheelers was developed and the dynamic simulation, hardware in the loop simulation (HILS) to evaluate the drive performance on motor dynamometer was conducted and the applicability of this simulation method was analyzed. First, we developed a new method to determine the road load occurring in a road drive, different from the coastdown test generally applied to vehicles. In our proposed method, the correlation between the speed and the road load is derived from fitting the motor's current consumption and speed while driving

at constant speed on a uniform horizontal road. Because the inertial resistance is almost negligible while the vehicle drives at constant speed on a uniform horizontal road, the output of the engine or drive electric motor is the same as the running resistance. The output torque of drive motor of electric two-wheeler is proportional to current consumption and this linear coefficient is expressed by k_t, torque constant. So the running resistance of electric two-wheeler driving at constant speed on a uniform horizontal road can be determined by measuring the current consumption of electric two-wheeler's drive motor and calculating the drive motor's output torque. The correlation between the output torque and the current consumption was derived from the motor characteristic test on a motor dynamometer. And during the motor characteristic test and the real road tests the temperature of motor's windings was monitored so that the effects of the thermal equilibrium, saturation to the performance characteristics were evaluated. The difference between the road load which were derived in the case of the saturation state and non-saturation state respectively were 0.2 Nm. And the difference between the road load which were derived in the case of the non-saturation state and coastdown test was 1.0 Nm. If the new method is applied for determination of the road load, the road load can be determined through the new method though the coastdown test is not available for the regenerative braking when coasting.

Also it was ensured from the road tests that the new method needed driving tracks shorter than that in the coastdown tests. Second, we conducted HILS on a motor dynamometer by including real hardware to simulate the e-bike's field drive test, through which we verified the applicability of our new method. In order to apply the road load the test motor on motor dynamometer, the load machines are necessary for the dynamic simulations and the powder brake and servo motor were used for load machine on the separate test bed. On the motor dynamometer equipped with the powder brake, after the road load was calculated from the correlation between the speed and the road load obtained from the coastdown tests, the rodad load was applied to test motor through the powder brake by setting the above road load as the set value of the PI controller and comparing and compensating the set value and the present value. Because the powder brake can impose a passive load, it cannot operate at speed control mode. So the powder brake operated at torque control mode during the dynamic simulation. Unlike the powder brake, the servo motor can operate both at speed control mode and torque control mode, so the servo motor can impose a passive load as well as an active load. While the servo motor applied the road load to the test motor at speed control mode, the simulation was sequentially progressed calculating the dynamic equation based on the torque and rotational speed measured from the sensor and the

loop time. The powder brake and the servo motor included in the motor dynamometer simulated the road load derived from our proposed method and the coastdown test. If the dynamic simulation conducted in this study is applied for pre-evaluation of the drive module consisting of the motor, MCU, and battery, time, cost, and human resources necessary for the real road test being installed on the complete vehicles will be considerably reduced.

Keywords: Electric two-wheeler, Road load, Motor torque constant, Hardware in the loop simulation (HILS), Motor dynamometer

***Identification Number*: 2009-31242**

Contents

List of Figures

List of Tables

Nomenclature

$C_R(v)$	coefficient of rolling resistance, dependent on vehicle's speed, v
C_0	constant coefficient of $C_R(v)$
C_1	first-order coefficient of $C_R(v)$
C_d	coefficient of aerodynamic resistance
F	force [N]
I_{in}	input current at input terminal of MCU [A]
I_p	parasitic current in MCU [A]
I_w	current through winding of motor [A]
T	torque [Nm]
dv/dt	derivative of vehicle's speed, acceleration [ms-2]
g	gravity acceleration [ms-2]
k_t	torque constant of motor [-]
m	total mass, including e-bike, rider, and mobile data acquisition system (DAQ) [kg]
m_a	apparent mass of the e-bike [kg]
m_r	equivalent mass of the rotating parts of the e-bike [kg]
r	wheel radius [m]
v	vehicle speed [km h-1]
δ	efficiency of conversion of input current of MCU into winding current [-]
θ	angle of road slope [°]

Subscript

d	running resistance
e	output of engine (or electric motor)
nsat	non-saturation state of electric motor
sat	saturation state of electric motor

Chapter 1. Introduction

1.1 Background of the study

Environmental problems and the resulting need for alternative energy other than fossil fuels have propelled the active R&D and popularization of eco-friendly vehicles in recent times. The different types of eco-friendly vehicles include battery electric vehicle (EV), hybrid electric vehicle (HEV), and hydrogen fuel cell vehicle. To compete effectively with internal combustion (IC) engine vehicles in the automotive market, eco-friendly vehicles need to demonstrate verifiable equivalent or higher drive performance.

A vehicle's driving performance is characterized by its speed, energy efficiency, and climbing and acceleration abilities. These characteristics are tested and evaluated quantitatively using field or chassis dynamometer tests. Field tests offer improved accuracy and feasibility at the point of driving on a real road as compared to chassis dynamometer tests. However, uncertainties in the measurement and evaluation of a vehicle's performance in outdoor conditions such as wind, temperature, and humidity, and in unfavorable road conditions (such as roughness and irregular slope) can render field test results less reproductive and inconsistent. Consequently, field and chassis

dynamometer tests have a mutually complementary relationship, and it is important to impose the road load condition on a vehicle tested on a chassis dynamometer as precisely as the real driving condition as possible. Fig 1.1 shows the procedure to determine the road load through the field tests. After the determination of the road load and the deriving of the correlation between a speed and a road load are completed, setting a road load to chassis-dynamometer is implemented and then the driving performance evaluations are available on chassis-dynamometer. Coastdown test is the standard and most frequently used test for evaluating a vehicle's drive performance and determining its road load. Concrete and detailed studies on the coastdown test were commenced in the 1960s, following which related extensive studies, experiments, standardization, and mathematical and statistical analyses have been conducted and reported. Specifically, coastdown test conditions and methods for passenger cars and motor cycles have been established as international standards. [1] After obtaining the correlation between the speed and the road load, settings the road load on chassis-dynamometer and verifications of the reproduction are needed and the international standards gives detailed instructions on the methods of the chassis-dynamometer setting procedures. [2, 3] And the test methods about the drive performance of EVs and electric two-wheelers also have been established as international

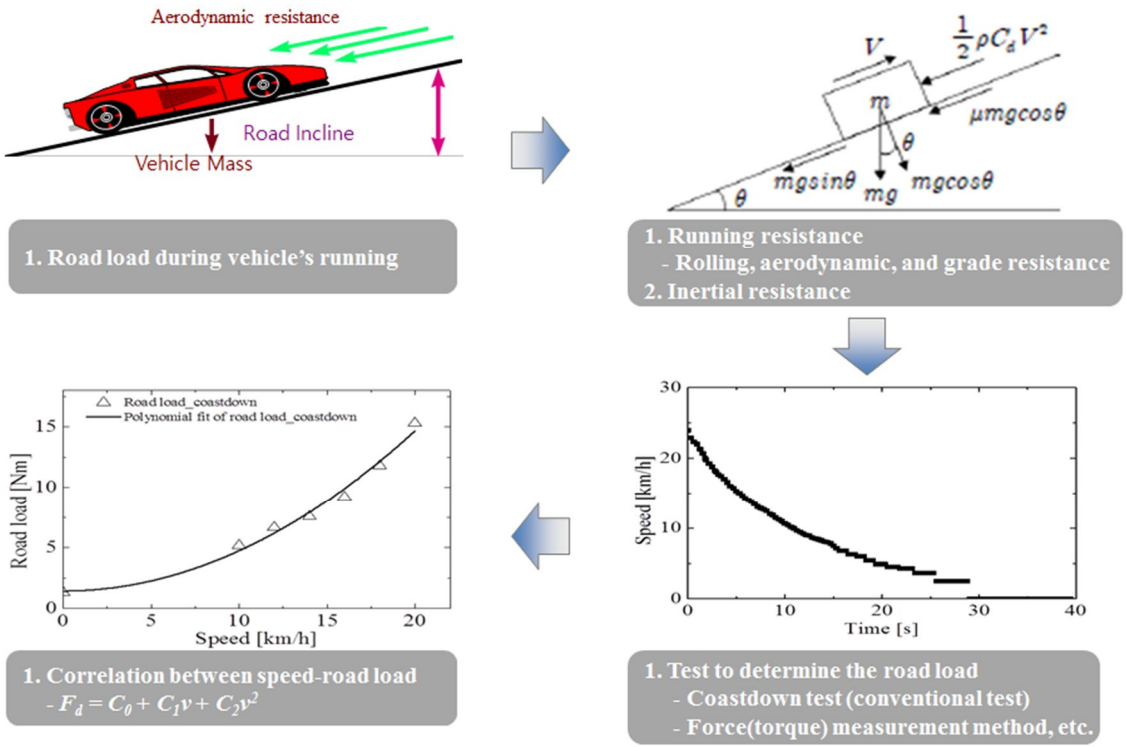

Fig. 1.1 Procedure to determine the road load through the field tests

Table 1.1. Test method standards about the drive performance of EVs and measurements and setting of road loads

Items	**Standard numbers**	**Standard names**
Test method about the drive performance of EVs		
ISO	8714: 2002	Electric road vehicles - Reference energy consumption and range -- Test procedures for passenger cars and light commercial vehicles
	8715: 2001	Electric road vehicles -- Road operating characteristics
	13064-1: 2012	Battery-electric mopeds and motorcycles - Performance - Part 1: Reference energy consumption and range
	13064-2: 2012	Battery-electric mopeds and motorcycles -- Performance -- Part 2: Road operating characteristics
Test method about the measurements and setting of road load		
ISO	10521-1: 2006	Road vehicles - Road load - Part 1: Determination under reference atmospheric conditions
	10521-2: 2006	Road vehicles -- Road load -- Part 2: Reproduction on chassis dynamometer
	11486: 2006	Motorcycles -- Methods for setting running resistance on a chassis dynamometer

standards. [4-7] Table 1.1 lists the details of these international standards.

The road load of a motor-driven EV can also be tested and determined using the coastdown test. However, most studies on using this test to determine road load have been limited to IC engine vehicles. Paper search and literature review yielded few studies on using coastdown tests for EVs. Therefore, the first subject of this study is about a new method, different from the coastdown test, to determine the road load of an EV by measuring the current consumption in the drive motor when the EV is running at constant speed. In the case of motors like BLDC motor which has a constant magnetic flux, for example by using the permanent magnet, the current through motor windings is linearly proportional to the output torque of the motor by a coefficient known as the torque constant k_t *[8]*. The torque constant k_t, is an important motor design factor, and unique and invariable once the motor's specification is decided.

We verified the proposed method by comparing results of the field test and dynamic simulation. The dynamic simulator comprises a control and monitoring system, a vehicle drive module (motor, MCU, and battery), and a motor dynamometer equipped with a powder brake.

The second subject of this study is about the dynamic simulation to evaluate the drive performance of EVs that is implemented on motor

dynamometer including the real hardware like the drive motor, MCU, and battery. In general, the simulation methods which insert the real hardware in the simulation loop and interact with the theoretical logic are known as the hardware in the loop simulation (HILS). While the conventional simulation mostly consists of the computational logics based on the personal computer, HILS has additional components, real hardware focused on evaluation besides the conventional simulation. HILS can be used for the purpose that the prototype of complete products will be pre-evaluated and the performance and the reliability is need to be verified before the complete products are supposed to make. Also HILS has an advantage that the costs and human resources for research and development of the products can be considerably reduced. In this study, HILS was implemented on two motor dynamometers equipped with the powder brake and the servo motor, respectively in order to simulate the driving condition on real road on laboratory.

The types of HILS performed in the fields of electric drive motor and IC engine development can be divided into three types according to the level at which they are conducted: the signal level, the power level, or the mechanical level. [9, 10] Fig 1.2 shows the examples of the three types HILSs about testing the electric motor. Wu et al. [11], Ramaswamy et al. [12], Kim et al. [13], Kwon et al. [14], and Yoon et al. [15] studied the use of HILS at

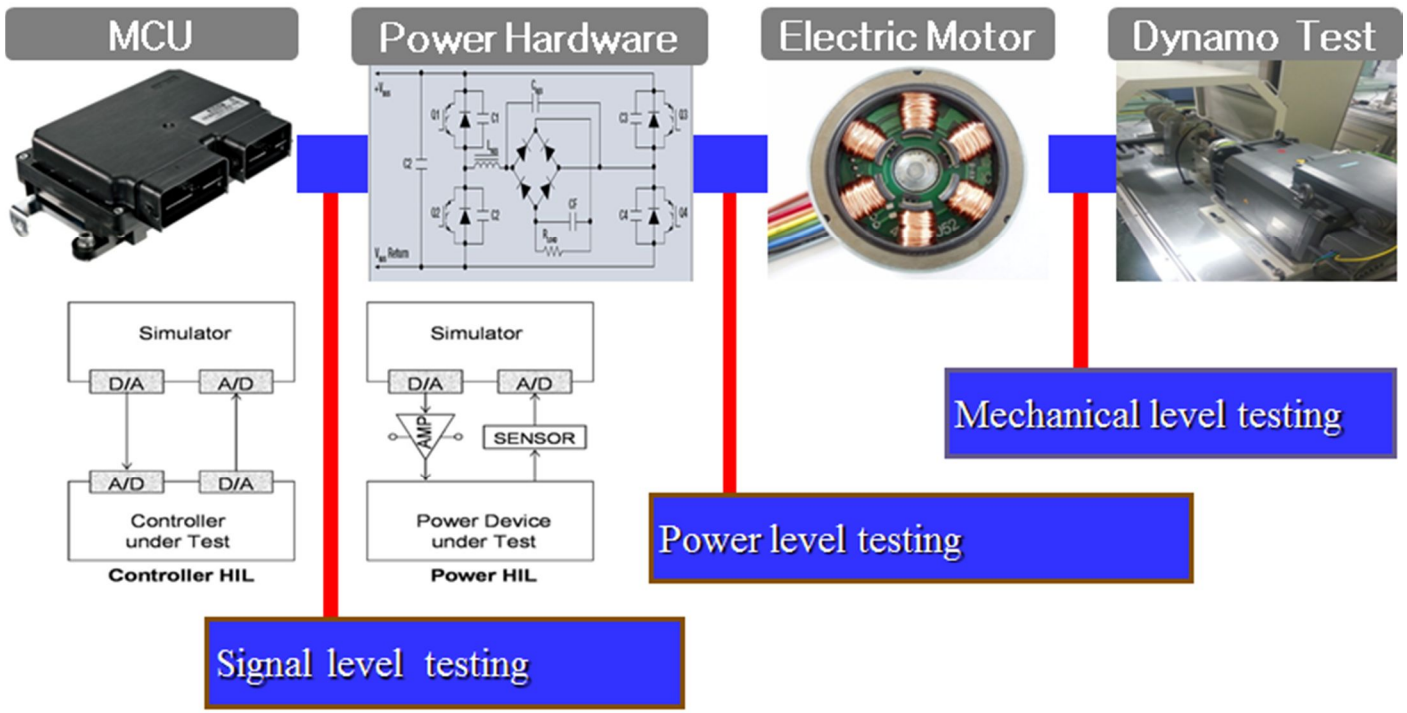

Fig 1.2 Examples of the three types HILSs about testing the electric motor (National instrument, [16])

the signal level. For example, Yoon et al. [15] performed a dynamic simulation of an HEV drive motor using an HILS for the purpose of pre-performance evaluation of an MCU's reliability at a motor drive pulse width modulation (PWM) frequency of 20 kHz. In HILS at the power level, actual power electronics such as inverters are evaluated, and the other parts (the electrical machine and mechanical load) are simulated. [17, 18] In HILS at the mechanical level, such as that performed in this study, actual electric motors or engines are applied to the mechanical load and evaluated under simulated conditions. [19-21] For example, Lin et al. [20] developed and verified a dynamic simulator consisting of an engine, a transmission, and a fuel and air injection system to conduct a dynamic simulation of a motor dynamometer by applying a road load to an IC engine through a powder brake. While their study dealt with HIL tests of an IC engine and very precisely simulated field tests of a motorcycle, the road load of the motorcycle was determined on the basis of a numerical calculation technique called a bond-graph technique, rather than on the basis of a coastdown test, and the inertial resistance was implemented somewhat incorrectly because the inertia of the flywheel used in the HIL test set-up deviated insufficiently from the real inertia of the motorcycle.

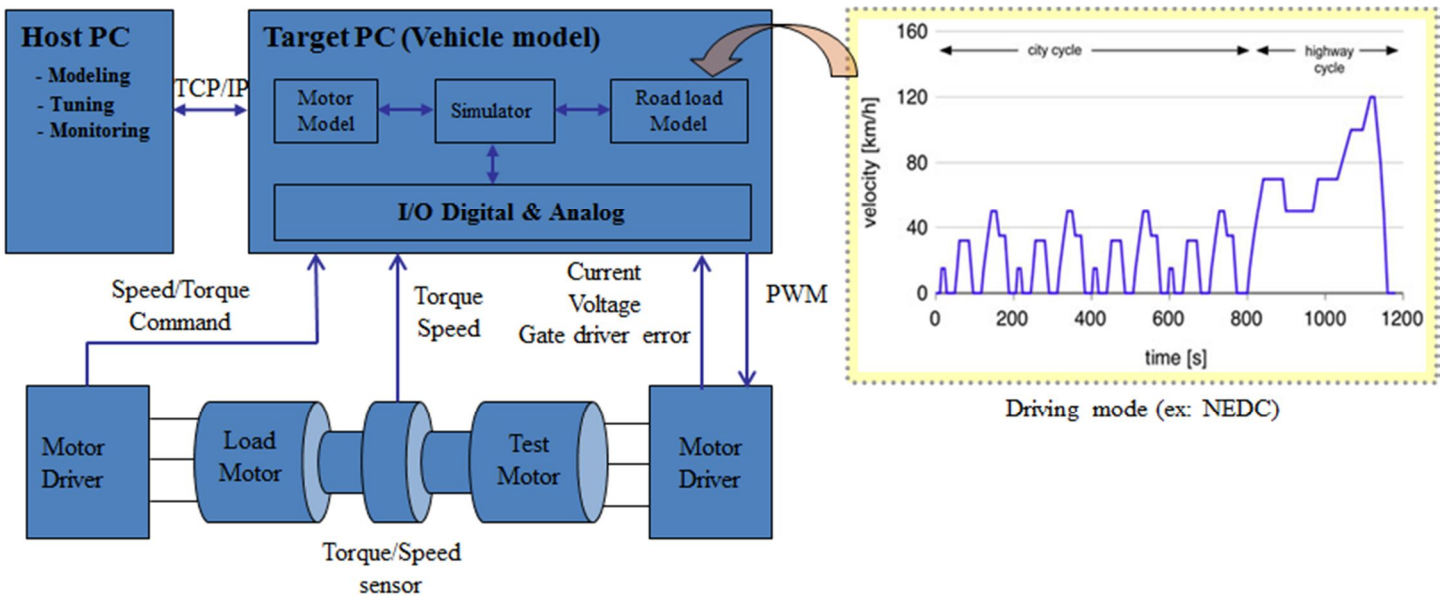

Fig 1.3 Schematic diagram of the HILS at the mechanical level to evaluate the electric motor's performance

Fig 1.3 illustrates the schematic diagram as the example of the HILS at eh mechanical level to evaluate the electric motor's performance. In this simulation, many types of transient and fault conditions on test motor that are difficult or impractical to perform with real systems by using the latest technology for real-time high-fidelity electric motor simulation. [16]

The novel method to determine the road load was performed riding e-bike in the real road. The test e-bike is installed with a 250-W-class brushless DC (BLDC) motor and a lithium-ion battery. During the field test, we rode the e-bike using only the electric motor drive without pedaling or regenerative braking. The e-bike belongs to the renowned e-mobility technology that electrically powers vehicles for short-distance commuting and transportation for work [22, 23]. E-mobility includes e-bikes, electric scooters, electric wheelchairs, and all-terrain vehicles (ATVs).

We expect our proposed method will be good comparison with the conventional coastdown test through mutual comparative analysis. If there is a case that coastdown tests are hard or impossible to apply when determining road load, for example in the case of EVs having the function of the regenerative braking, our proposed method can be considered to be a good alternative.

1.2 Literature survey

As commented in previous chapter, lots of studies on the drive performance of eco-friendly vehicles are available in literature. Coelho and Karner studied the drive performance characteristics (such as energy consumption efficiency and battery capacity) of HEVs using on-board measurement and a chassis dynamometer [24, 25]. Howey gathered energy consumption data for electric, hybrid electric, and IC vehicles in real road conditions, which revealed that EVs used the least amount of energy [26]. Wager tested energy efficiency and driving range of EVs in relation to gear selection using a chassis dynamometer and he said in conclusion that following EV test standards needed attention to detail in meeting drive cycle parameters. And the drive cycle parameters might include the coefficients for road load though he didn't directly mention those.

The drive performance of EVs can be evaluated in field testing and chassi dynamometer testing. In order to make the test results consistent and reproductive, chassi dynamometer testing generally is adopted in the field of the vehicle performance tests. And it is very important that the road load is accurately imposed on the vehicle mounted on chassi dynamometer as if the vehicle is driven on the real road. To determine the road load which needs to be set on the chassi dynamometer is conducted through the coastdown test

during the deceleration of the vehicle.

1.2.1 Test method to determine road load

The active and extensive studies on coastdown tests were commenced in 1960's. As a lot of effort to improve the drive performance of vehicle was made, the empirical and statistical studies on coastdown test were actively done in order to accurately measure the vehicle's road load. Cenek performed coastdown tests on vehicles installed with onboard anemometers and road slope measurement systems, and comprehensively summarized the effects of road surface properties, interactions between the tire and the road, and relation between coefficients of rolling and aerodynamic resistances on the road load *[27]*. Roussillon obtained a realistic measure of C_D from deceleration tests in light cross-wind on a track having slight gradient by considering velocities relative to the track and to the wind. He said it was possible to establish energy balances and correlation between wind-tunnel and real road from his experimental measurements. Swift analyzed the correlations between speed and road load using mathematical and statistical methods *[28]*. He said that optimal values of the related rolling resistance and drag coefficients for a given data set were found from a non-linear least-squares fitting procedure, and also overall confidence limits on the coefficients might be reduced by

averaging values over many separate runs. Carlson et al. conducted coastdown testing and chassis dynamometer testing of three vehicles, each at multiple test weights, in an effort to determine the impact of a vehicle's mass on road load force and energy consumption. The results of the testing and analysis showed that for a given vehicle, the road load shows a slightly non-linear trend of decreasing road load with decreasing mass.

1.2.2 HILS of vehicle drive performance

In our study, we have introduced the dynamic simulation which includes the real hardware existing in real environments in order to verify the feasibility and compatibility of our proposed method to determine the road load and perform the pre-evaluation of the EVs prior to the production. Through our dynamic simulation, it is possible to evaluate the performance o the drive motor, the battery and the other comprising parts of EVs without the complete set up of the vehicle and the surrounding environments. Our dynamic simulation is similar to the hardware in the loop simulation, HILS in the point of the above functional properties. But while HILS possesses the characteristics like the synchronization and real time operation by adopting the micro controller designed for embedded applications, the dynamic simulation of our study just used the application based on Labview which

enabled the data measurements and control assignment like PI control for the ultimately short period in orders of micro seconds. In extensive fields of electrics, transportations, and engineering fields etc., the dynamic simulations including HILS are applied nowadays. Lin et al. developed and verified a dynamic simulator that simulated the field test of an IC engine motor cycle. This simulator, which comprised an engine, transmission, and fuel and air injection system [20], was used to conduct dynamic simulation on a motor dynamometer by applying road load to the IC engine through the powder brake. Yoon et al. performed the dynamic simulation of an HEV drive motor using a hardware-in-the-loop simulation for the purpose of pre-performance evaluation [15] of its reliability under the condition that the pulse width modulation (PWM) frequency of the motor drive was 20 kHz. He et al. carried out the HILS containing the hybrid power/energy system to verify the energy management strategy under the Urban Dynamometer Driving Schedule(UDDS) dynamic driving cycle. Their results showed the proposed fuzzy logic-based energy management strategy can ensure the battery pack working in high efficiency range and showed better performance than the traditional logic threshold-based control strategy.

1.3 Objectives and scopes

The objectives of this study are the development of the new method to determine the road load of EVs unlike the coastdown test generally applied to vehicles and the development of the dynamic simulator to reproduce the real driving conditions of EVs on motor dynamometer at laboratory. EVs have distinct and intrinsic features separated from IC engine vehicles, which mainly issue from the power source like battery and fuelcell and the electric motors for traction force. Our proposed method uses the characteristics of the electric motors that the output torque is proportional to the current through the windings in the case of the constant magnetic flux like the permanent magnet in BLDC motors. Though the empirical validation was carried out on a e-bike, our proposed method can be applied to the general EVs and considered as the compatible alternative to the coastdown test, because the e-bike is the subcategory of the EVs and we just used the characteristics of electric motors, BLDC motors which can be applied in the general EVs.

And the dynamic simulator for evaluating the performance of the drive motor of the electric vehicle based on the HIL testing techniques was introduced and studied using the motor dynamometer equipped with the powder and the servo motor.. When considering the cost, time, test coverage range, etc. in the evaluation of the driving module of the electric vehicle,

applying a dynamic simulator introduced in this study will be a very effective testing and evaluation procedures. Two dynamic simulators were constructed on dynamometers equipped with a powder brake and a servo motor as load machine, and the simulation results were analyzed to reproduce the performance of the actual driving conditions of the e-bikes through the comparison of the real road test.

In chapter two, the novel method to determine road load was introduced and test results about the relation between motor current consumption and road load was shown and discussed. we perform the motor characteristic test on motor dynamometer in order to find the torque constant, k_T of the drive motor. In tests, we measured the current, voltage, rotating speed of motor, and torque through DAQ and sensors on motor dynamometers. Test results show the linearity between the output torque and the current into MCU is valid for the drive motor of the e-bike.

Prior to the explanation of the field test, the dynamic equation in EV while driving at constant speed was introduced, and this equation was applied to derive the coefficients of road load for rolling resistance and aerodynamic resistance. Riding an e-bike at constant speed on a horizontal road, we obtained the time-current and speed profiles for 6 references speeds. From the least square fitting procedure, the 2^{nd} order polynomial equation of road load

was found.

In chapter three, the dynamic simulation under torque control mode on motor dynamometer combined with the powder brake was introduced and the test results of dynamic simulation and field test were analyzed and compared together. The virtual environment for the drive in real road was constructed by imposing the friction torque on the drive motor through the powder brake of the motor dynamometer. The dynamic simulator included the two P-I controller for the motor's speed and the road load.

In chapter four, the dynamic simulation under speed control mode on motor dynamometer combined with the servo motor was introduced and we simulated the driving conditions on motor dynamometer about the coastdown and the acceleration from the standstill in real road. After the field tests and the dynamic simulation on motor dynamometer, we verified the fidelity and the reproducibility of the developed dynamic simulator using the servo motor type motor dynamometer.

Finally, the concluding remarks are given along with the brief summarization of results and discussions.

Chapter 2. New torque-speed balance method to determine road load

2.1 Introduction

Active efforts to reduce greenhouse gas emissions for preventing global warming have also been underway in the global automotive industry. There are many reasons to improve the fuel efficiency of vehicles, one of which is to decrease greenhouse gases by reducing CO_2 emissions per km. As for the running performance of the vehicle, including fuel efficiency, it is important to perform tests and evaluations in accordance with objective criteria. In general, an evaluation on the running performance of the vehicle is made through the chassis dynamometer installed in the laboratory, and the road load measurement is essential to reproduce the running state of the vehicle on a chassis dynamo.

Among methods for measuring the road load of the vehicle, coastdown test is most widely known, and there is a force (or torque) measurement method as a comparative test method with the coastdown test. The force measurement method is designed to measure the road load applied to a tire directly by mounting a torque sensor to a wheel. This method has the

advantage of being able to measure the road load except for drive train loss from the power source such as engine and motor to the wheel. However, it poses the disadvantage that wheel torque sensor is expensive and difficult to install. [29-32] In addition to this, Pascoa et al. devised a method to obtain the aerodynamic resistance using an aerodynamic shield and a separate car to tow the test vehicle. In their study, the aerodynamic resistance coefficient was obtained by towing the vehicle with and without an aerodynamic shield, in order to eliminate the rolling resistance component.[33] Bonhomme et al. devised a method to measure the rolling resistance using a uniaxial testing machine. A new test configuration to measure the coefficient of rolling resistance with uniaxial mechanical testing machines has been presented. [34]

Until now, it's true that most studies on experimental method to determine road load have been limited to internal-combustion engine vehicles and paper and literature reviews yielded few studies on using coastdown or similar tests for EVs including e-bike. In this chapter, we intend to propose a new method, different from the coastdown test, to determine the road load of an e-bike by measuring the current consumption in the drive motor when the e-bike is running at constant speed. In the case of motors like brushless DC(BLDC) motor which has a constant magnetic flux, for example by using the permanent magnet, the current through motor windings is linearly

proportional to the output torque of the motor by a coefficient known as the torque constant k_t [8]. And the torque constant is an important motor design factor, and unique and invariable once the motor's specification is decided. In our proposed method, we applied dynamic equilibrium to an e-bike which had an in-wheel drive motor and was running at constant speed on a horizontal road in the longitudinal direction. In this dynamic equilibrium, the road load as a combination of rolling and aerodynamic resistances equals the output torque of the drive motor, which is the torque constant times the current consumption.

The novel method to determine the road load was performed riding e-bike in the real road. The e-bike is considered to be the subcategory of EVs, but there are three main differences between test e-bike and EVs. The first difference is the drive motor's type. While test e-bike is equipped with BLDC motor, electric motors for EVs include AC motors like induction motors as well as DC motors like BLDC motors. In the case of BLDC motors, the linearity between torque and current is valid regardless of the speed of the motor due to the constant magnetic flux in rotor or stator. But this linearity between torque and current according to speed variation of the motor is not compatible with AC motors because of the differences in structure and operating principle [35, 36]. The second difference relates to drive mode

based on power transmission systems. The driving modes of the EVs include traditional driving mode, motor-drive axle combined driving mode, motor-drive axle integrated driving mode and wheel driving mode [37]. Among the above drive modes, test e-bike uses wheel driving mode that the motor are installed in the wheel and doesn't have any power transmission system like clutch, shaft and differential transmission systems. In wheel driving mode, there is no loss of power through the transmission system, because the output force of the drive motor is directly transferred to the surface of the road. The final difference is regarding the use of regenerative braking. In general, EVs have the function that the kinetic energy during coasting and braking modes generates electricity back to the supply side, and this is known as regenerative braking [38]. Test e-bike doesn't have the function of regenerative braking. If regenerative braking operates when an EV is coasting, it is almost impossible to make an accurate measurement of road load. So an additional work to remove the function of regenerative braking must be performed before coastdown testing of EVs.

Taking the above statements into consideration, our proposed method can be applied to EVs which have following two characteristics.

1) EVs installed with drive motors possessing the linearity between torque and current regardless of the speed of the motor.

2) EVs using the wheel driving mode with no transmission system between wheels and power source.

We verified the availability of proposed method by comparing results of the coastdown test and the new method. We expect our proposed method will be good comparison with the conventional coastdown test through mutual comparative analysis. If there is a case that coastdown tests are hard or impossible to apply when determining road load, for example in the case of EVs having the function of the regenerative braking, our proposed method can be considered to be a good alternative.

2.2 Dynamic equation in EV while driving

The coastdown test involves a consecutive procedure including acceleration of the vehicle to as high a speed as practicable, disengaging from transmission, setting in neutral positions, and allowing the vehicle to coast to a low speed without any drive power. The time-speed profile is obtained by simultaneously recording time and vehicle speed, and using this profile, the relation among speed, rolling resistance and aerodynamic resistance is determined. During driving, the vehicle is subjected to a road load, which consists of running and inertial resistances. Running resistance, in turn, comprises rolling, aerodynamic, and grade resistances as in equation (2.1).

$$F_e - F_d = F_e - C_R(v)mgcon\theta - C_D v^2 - mgsin\theta = (m+m_r)dv/dt = m_a\, dv/dt \qquad (2.1)$$

$$C_R(\mathrm{v}) = C_0 + C_\mathrm{n} v^\mathrm{n} \qquad (2.2)$$

where $C_R(v)$ is the coefficient of rolling resistance dependent on speed with the order n = 1 (linear) or n = 2 (quadratic). [28] In our study, we adopted the linear coefficient for $C_R(v)$. And m_a is the apparent mass of vehicle that includes the total mass of vehicle and the equivalent mass of the rotating parts kinematically connected with the wheels. In the point of the kinetic energy conservation, the vehicle behaves as having a bigger mass, the apparent mass [39].

The coastdown test requires the measurement of $\Delta v/\Delta t$ under the condition $F_e = 0$, whereas in our study, we need to measure the current consumption of the e-bike resulting in F_e under the condition $\Delta v/\Delta t = 0$. Through this method, we can determine $C_R(v)$ and C_D by regression analysis for more than four reference speeds. Our study is based on the linearly proportional behavior of the output torque to the current through the winding, resulting in equation (2.3).

$$T_e = rF_e = k_t I_w \qquad (2.3)$$

where k_t is the torque constant determined from the motor characteristic test on the motor dynamometer. We assume that the input current into the MCU comprises the current through the winding with conversion loss, and the parasitic current necessary for operating the MCU's electronic parts and the e-bike's throttle unit. Hence, we determine the current through the winding from equation (2.4).

$$I_w = \delta I_{in} - I_p \tag{2.4}$$

The above correlation is assumed to be valid for every motor and MCU of the same lot and specification.

If the e-bike is driven at constant speed on a uniform horizontal road ($\theta \approx 0$) on a calm and windless day, the movement equation of the vehicle, equation (2.5) will be satisfied.

$$F_e - F_d = F_e - C_R(v)mg - C_D v^2 = ma\ dv / dt = 0 \tag{2.5}$$

$$F_e = (k_t I_w) / r = (k_t(\delta I_{in} - I_p)) / r = C_R(v)mg + C_D v^2 \tag{2.6}$$

We conducted field tests with the e-bike for more than four reference speeds

and determined $C_R(v)$ and C_D values by least-squares regression analysis using field test results.

2.3 Motor characteristic test on motor dynamometer

The test e-bike is equipped with an in-wheel motor that shares its shaft with the wheel and has a rotating outer housing connected by a rotor. It is not easy to install the torque sensor in the vehicle and measure the output torque of drive engine or motor when the vehicle is running on the road because of the limited and harsh spaces for the torque sensor. The current sensors have an advantage over torque sensors regarding installment and handling on vehicle. So in this study, we measure the current consumption of the drive motor so that the output torque of the motor subsequently is derived when driving on the road. The relation between the current consumption and the output torque was derived from the motor characteristic test performed on the motor dynamometer.

The characteristics of the electric motors including BLDC motors can be represented by the profiles of the parameters like power, current, and torque according to the rotating speed. Generally, dynamometers or brakes are commonly used to measure the motor torque-speed characteristics for performance assurance and this approach is defined as direct measurement by

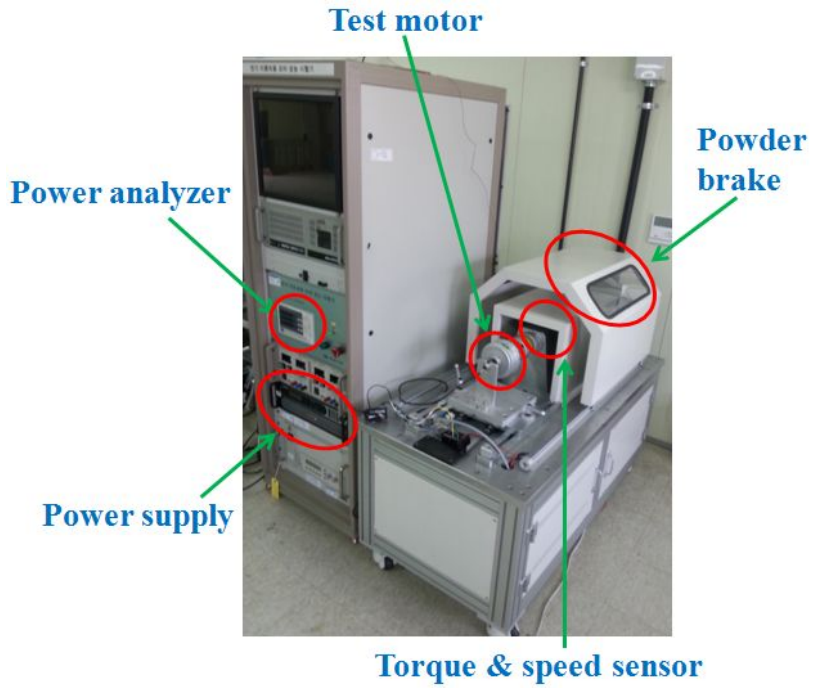

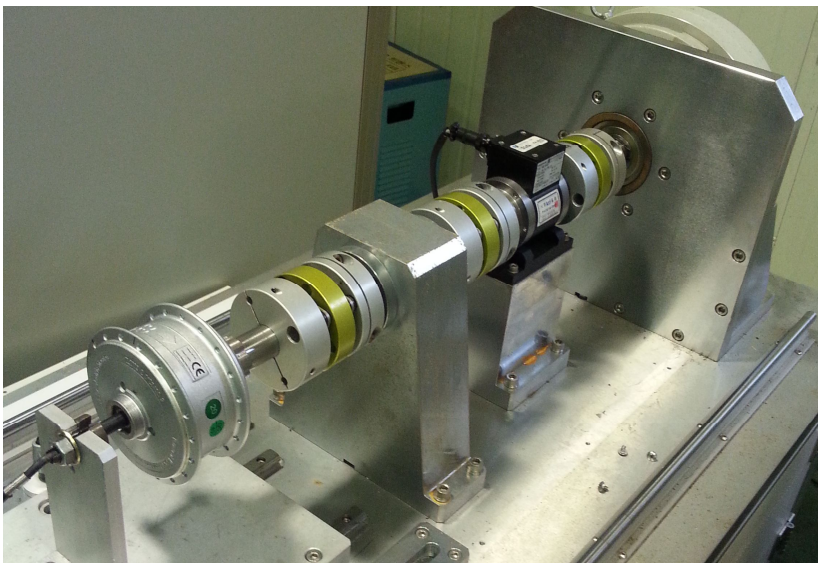

Fig 2.1 Motor dynamometer and its comprising parts.

IEEE. [40] Also International standard test procedures for torque-speed tests of kinds of electric motors were reported in [41], [42], and [43].

In order to find the torque constant of the motor, we selected the same motor and MCU as those installed in the e-bike, and assumed that both motors and MCUs have the same torque constant. Subsequently, we conducted the motor characteristic test on the motor dynamometer shown in Fig. 2.1, which is coupled with the drive motor of the test e-bike. During the characteristic tests, the temperature of motor's inner windings was monitored indirectly by measuring the temperature of the phase line outside of the motor housing in order to look into the aspects of motor's saturation. So the characteristic curves according to the saturation and non-saturation states were acquired, respectively. From the test, we derived the torque constant and the characteristic curve representing torque-rpm and torque-current relations. The throttle device assigned to the MCU as the instruction command for the motor to operate and rotate was fixed at fully rotated state during the characteristic test.

2.3.1 Experimental setup

The motor dynamometer mainly comprises a powder brake, power supply and measurement and control parts including sensor and analyzer parts

for torque, rotating speed, voltage, current, and power, as indicated in Fig. 2.1. Table 2.1 lists the specifications of the motor dynamometer. The powder brake, rigidly coupled with the motor's shaft, applies mechanical braking force to the test motor by electromagnetic reaction so that road load acting on the e-bike during the drive can be properly simulated. Its output and braking force were controlled linearly by applying an analog voltage of 0–10 V assigned to the brake power supply. The measurement and control parts were set up using a personal computer (PC), the DAQ, and a software program based on LabView. The TM-311 torque transducer from Magtrol for sensing torque and rotating speed was mounted between the test motor and the powder brake. The motor's current consumption, voltage, and power at the input terminal of the MCU were measured using the power analyzer. And the temperature of the motor winding was measured at an insulated surface on a power line of 3 phases into the motor housing by using the T-type thermocouple.

And the analog voltage signal assigned to the MCU as the instruction command for the motor to operate and rotate was fixed at 3.5 V during the characteristic test. Beginning from a no-load condition, as we applied increasingly greater load on the motor using the powder brake, we derived the relation between the torque and the current consumption.

And as shown in Fig 2.2, it is the attentive point that the DC power

supply is used for power source during the characteristic test whereas the battery of the test e-bike is used for power source during the dynamic simulation. In characteristic tests on motor dynamometer, the supply voltage should be the same on every case because the different supply voltage causes the motor to rotate in a different speed. The motors are supposed to rotate in the way that the back electromotive force due to the rotating flux willingly approaches to supply voltage and is in equilibrium potential.

Table 2.1. Specifications of motor dynamometer.

Powder brake	
Model (Manufacturer)	ZKB-20XN (Mitsubishi)
Torque range	0–200 Nm
DAQ	
Model (Manufacturer)	PCI-6229 (National instruments)
Torque/speed sensor	
Model (Manufacturer)	TM-311 (Magtrol)
Accuracy	± 0.1 Nm, ± 1 rpm
Temperature	
Type	T Type
Range	- 200 to 350 ℃
Accuracy	± 0.5 ℃
Power analyzer	
Model (Manufacturer)	WT230 (Yokogawa)
Accuracy	0.1% of the reading plus 0.1% of the range

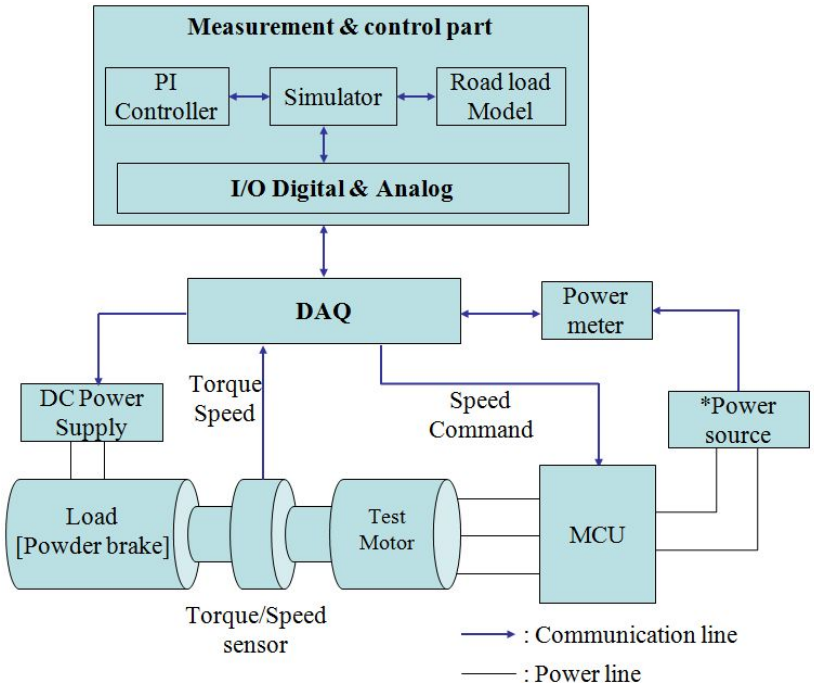

* Power source
: DC power supply when motor characteristic test
: Lithium ion battery when dynamic simulation

Fig 2.2 Schematic diagram of motor dynamometer for motor characteristic test and dynamic simulation.

2.3.2 Test results

Figure 2.3 and Figure 2.4 show the results of the characteristic test of the e-bike's BLDC motor in regard to torque, current and power according to speed and motor winding's temperature to check the saturation and non-saturation. The BLDC motor is the kinds of DC motors of which the general brush-type commutator is replaced with the switching devices like the transistor. So the BLDC motors have the similar features with the DC motors in the operating behavior on the torque, current, and speed. Beginning from a no-load condition, as we applied increasingly greater load on the motor using the powder brake, we derived the relation between the torque and the current consumption as shown in Fig 2.6. The motor was determined to be saturated if the temperature of windings wasn't increased by more than 0.5 K over 15 minutes. The non-saturated motor characteristic curve was acquired when the speed, torque and currents were steady over time regardless of the variation of the winding's temperature. As shown in Fig 2.3, the output torque and current is in inversely proportional to the rotating speed. The speed at no load was about 245 r/min. For overcurrent protection, it was found the current consumption of the drive motor didn't increase over about 10.7 A. And MCU controls the rotating speed of the motor being proportional to the input of the throttle in the hand grip which gives the analog voltage output from 1.4 to 3.5

V while spinning. In the characteristic test of the motor, we kept the output voltage of the throttle 3.5 V.

Figure 2.4 shows the motor characteristic curve for mechanical power-speed. The maximum power appeared to be 189 W when the speed reached about 186 r/min.

Fig 2.5 plots the current and the motor winding's temperature in the saturation state and non-saturation state. In order to compare the results, the temperature of the motor winding from the field test accurately, the temperatures of the surrounding area remained almost the same as about 28 ℃ while the motor characteristic test and the field test. As the loads increased from no load to about 10.7 A, the temperature of the motor winding also increased from 28.2 ℃ to 37.2 ℃ and from 29.2 ℃ to 42.9 ℃, at the non-saturation and saturation states, respectively. Because the temperature of the motor winding increased from the temperature at the non-saturation state to temperature at the saturation state, it was ensured that the temperature differences between at the non-saturation and saturation states increased from 1.0 ℃ to 5.7 ℃.

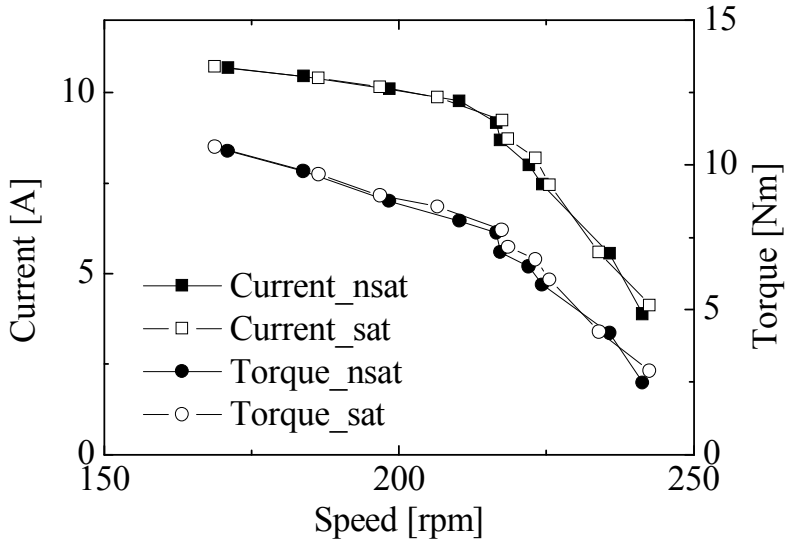

Fig 2.3 Motor characteristic curve for torque-speed and current-speed

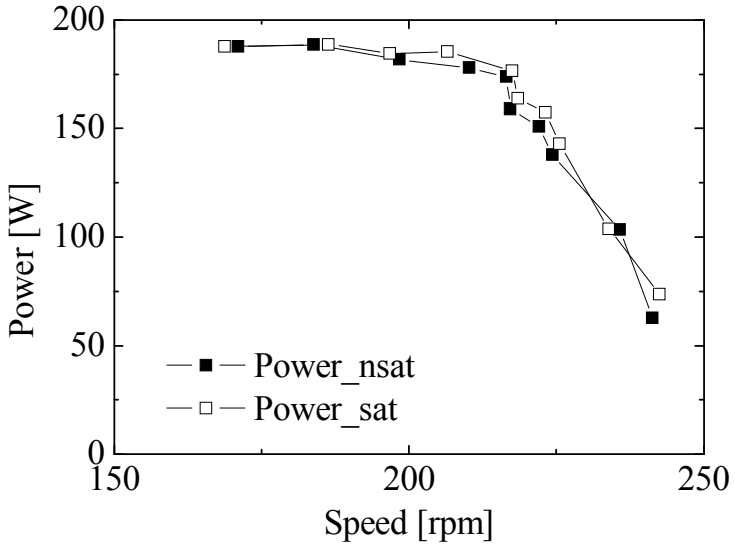

Fig 2.4 Motor characteristic curve for mechanical power-speed

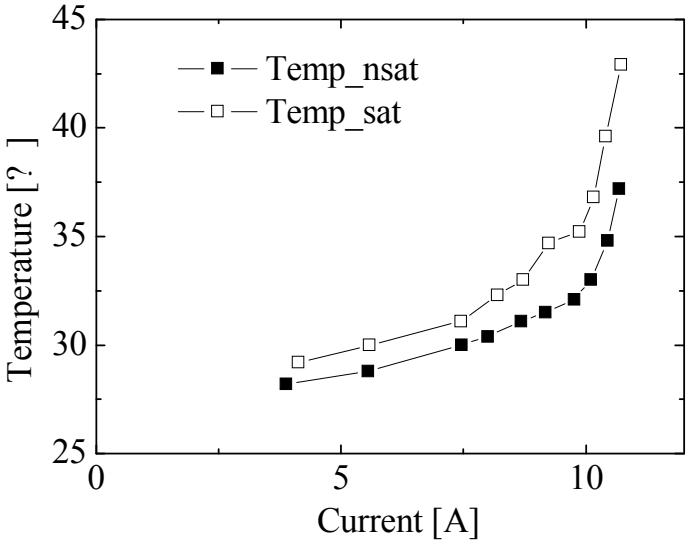

Fig 2.5 Plot of current-motor winding's temperature in the saturation state and non-saturation state

2.3.3 Correlation of current consumption and motor's output torque

By regression analysis, we obtained the following interaction equations between the torque and the current consumption of the motor according to the saturation state and non-saturation state.

$$T_{e,\,nsat} = 0.9559 I_{in} - 1.1976 \quad (I_{in} \leq 9.86) \tag{2.7}$$

$$T_{e,\,nsat} = 2.6754 I_{in} - 18.15 \quad (I_{in} > 9.86)$$

$$T_{e,\,sat} = 0.9459 I_{in} - 1.0276 \quad (I_{in} \leq 9.80) \tag{2.8}$$

$$T_{e,\,sat} = 2.4787 Iin - 16.052 \quad (Iin > 9.80)$$

The reason that the slope of the interaction equation varied from more than about 9.8 A was that the MCU had a function to prevent an overcurrent for safety and limited the motor's current consumption from the set overcurrent.

Owing to difficulties in measuring the current through the motor's winding due to the limited and harsh placement of the current sensor in the e-bike, we decided to measure the input current through the MCU. There were the y-intercepts, -1.1976 and -1.0276, because of the current loss during

conversion in the MCU and generation of parasitic current besides the current through the motor winding.

It is observed that the function of MCU for overcurrent protection about 13.2 A, is implemented as shown in Fig 2.6. MCU should not allow the drive motor to consume the current over the specific amounts against the safety accidents like electrical or physical malfunctions and consequent overheating etc. So though the load torque of the drive motor gradually increases, the current consumption of the drive motor doesn't increase above about 13.2 A. Besides the overcurrent protection function, the MCU of the e-bikes should have the additional safety functions such as low voltage protection and the phase short protection.

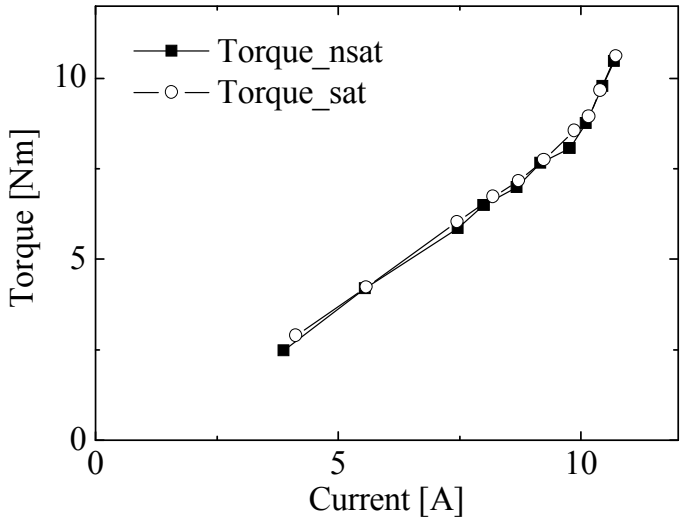

Fig 2.6 Motor characteristic curve for torque-current consumption.

2.4 Field test

The test e-bike is installed with a 190-W-class brushless DC (BLDC) motor and a lead acid battery. Specifications of the battery, motor and e-bike used in the real road test are shown in Table 2.2. The photos of the e-bike equipped with a mobile data acquisition unit(DAQ) and a mobile DAQ and its comprising parts such as current sensor and GPS are shown in Fig 2.7 and Fig 2.8. The real road test was conducted in a flat asphalt road on a windless day. During the field test, we rode the e-bike using only the electric motor drive without pedaling or regenerative braking.

In field test, we gathered the battery voltage, the battery output current, the throttle output voltage, the e-bike's speed using the mobile DAQ and the motor winding's temperature. National Instrument's cRio-9022 was applied to mobile DAQ for data acquisition. Battery voltage and output voltage of current sensor, LEM's HAIS50-P, was measured directly with an analog input module of the cRio, and battery output current was measured using a LEM's HAIS50-P current sensor. The Lowpass filter provided by the Labview was applied to the cRio's FPGA module to remove the high-frequency noise that appears in the output signal of the current sensor and battery voltage signal. The speed of the e-bike was measured in two ways, the GPS and monitoring the wheel's rotational speed by using magnets. The first method

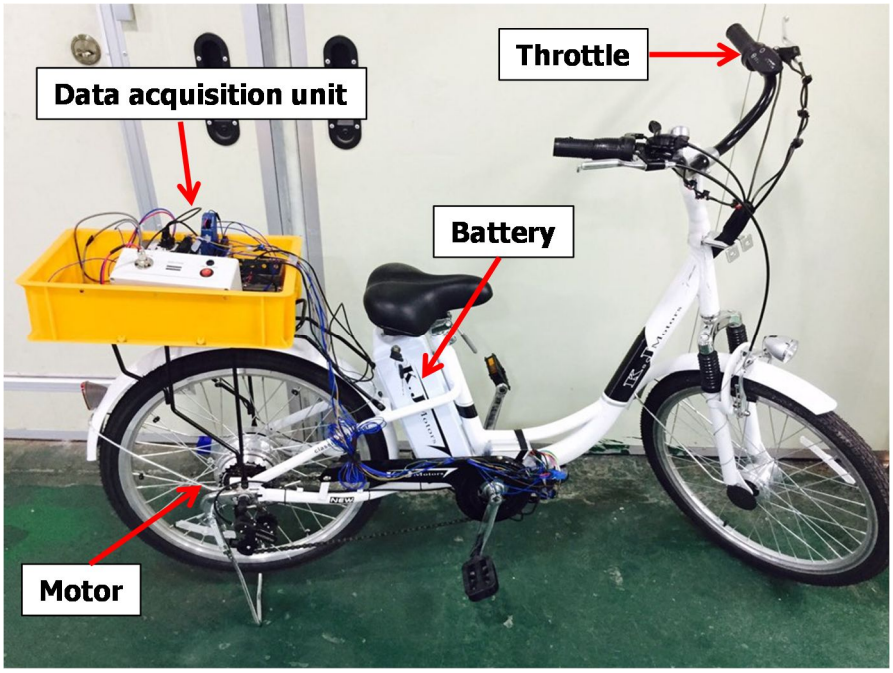

Fig 2.7 Picture of the test e-bike and mobile data acquisition unit.

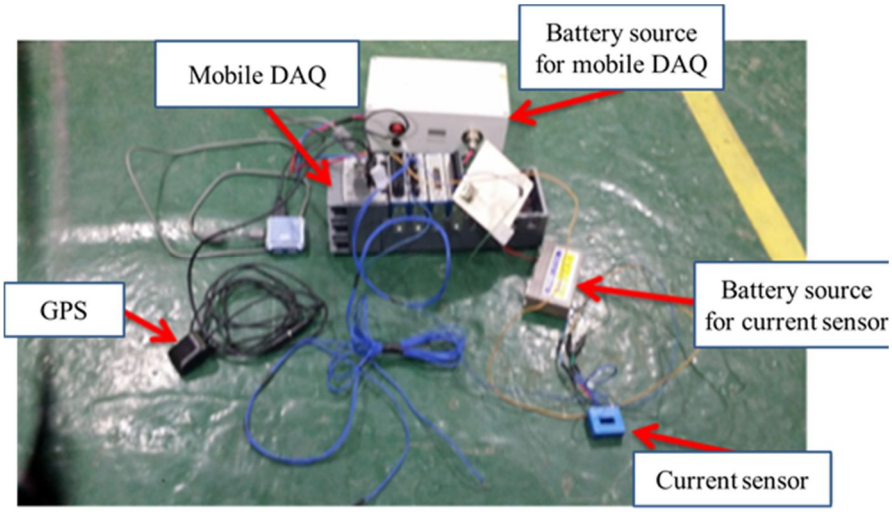

Fig 2.8 Picture of the mobile DAQ and the measurement units.

Table 2.2 Specifications of e-bike, battery and test motor.

Parameter	Value	Unit
E-bike		
Weight	31.56	kg
Wheel radius	29.00	cm
Rider weight	44.00	kg
Mobile DAQ weight	3.10	kg
Regenerative braking mode	No	-
		-
Battery		-
Type of battery	Lead acid	-
Nominal voltage	24	V
Nominal capacity	12	Ah
Test motor		
Type	Brushless DC motor	-
Rotating part	Outer rotor	-
Rated output	190	W
Rated voltage	24	V
Rated rotating speed	170	rpm
Rotating speed at no load	245	rpm

was using 9 magnets installed on the rear wheel spokes, reed switch and pull-down resistor. The time interval between the high level signals captured in the reed switch by the magnetic field of the two magnets was measured using a digital input module of the mobile DAQ. The second method was using the GPS receiver's data that send the data including position, velocity, and time to the mobile DAQ through the serial communication in the protocol the National Marine Electronics Association (NMEA). The GPS receiver was the 631A model of ASCEN GPS and its update rate was 1 Hz. And the speed obtained from GPS data was used only for reference to make sure the availability of the wheel's rotational speed. The motor winding's temperature was measured by using the T type thermocouple in the same way as in the motor characteristic tests. We recorded the data at the sampling rate, 5 samples a second in the mobile DAQ.

2.4.1 Coastdown test

A coastdown test was conducted after reaching the maximum speed by pedaling up to approximately 27 km/h. Time-speed profile obtained after performing the coastdown test is shown in Fig 2.9. The following speed-road load correlation equation was calculated by obtaining the road load torque that corresponds to 10 reference speeds (22, 20, 18, 16, 14, 12, 10, 8, 6, 4 km/h)

based on the international standards regarding the coastdown of the motorcycle. [3]

$$T_d = 1.8561 + 0.0109v + 0.0185v^2 \quad (2.9)$$

In order to find the coefficient of road load from the coastdown test data, the least square regression analysis was used about 10 reference speeds. The regression analysis was carried out so that the coefficients of road load had positive values since the negative values were nonrealistic.

And after reaching the maximum speed, the total distance until the standstill could be calculated from the integration of the speed with time and that was approximately 97 m.

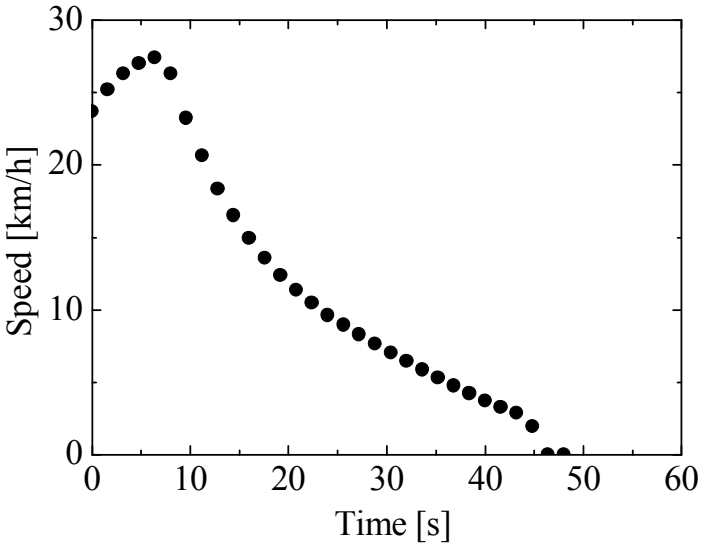

Fig 2.9 Picture of the test e-bike and its comprising parts.

2.4.2 New method under constant speed condition

Immediately after the coastdown, we performed the new method proposed in this study for the road load measurement. We gradually increased the speed by making the throttle yield the same output for 20 seconds or more, starting from a standstill, while driving approximately 280 seconds so that five constant speed sections can appear. Figure 2.10 and Figure 2.11 show time-speed/battery output current profile and time-motor winding's temperature/throttle output voltage profile, respectively. As shown in Fig 2.10, the battery output current is rapidly increased at the moment of acceleration, but is kept constant as the speed maintains constant. The measurement of the current sensor and the battery output voltage confirmed that the noise accompanied by a ripple occurs in the cruise control section with constant speed. This is a unique characteristic of the current sensor and voltage measurement module that also occurs in the laboratory test, and the noise was removed as much as possible using the lowpass filter applied to the FPGA module of cRio. With respect to the output voltage of the throttle, it was confirmed that the ripple is not relatively severe, but the intermittent ripple occurs.

The speed obtained from the wheel's rotational speed and the radius was verified by comparing the speed data obtained from the GPS data. Figure

2.12 shows the plots indicating the time-speed profile obtained from the wheel's rotational speed and GPS data. As shown in Fig 2.12, two time-speed profiles were almost similar in the sections of more than about 15 km/h. In the sections of less than 15 km/h, the tendency to increase of the speed from standstill was similar, but it was found that the speed of GPS was smaller than the speed obtained from the wheel's rotational speed. This was because the accuracy of the speed calculated by GPS signals declined with lower speed and the signal of GPS wasn't recognized at starting for the low position accuracy of about 3 m. And during constant speed drive, for example, 22 km/h, for 10 seconds, the total distance to an end was about 61 m. Comparing the total distance required in coastdown test, 97 m, the new method proposed in this study has an advantage that the shorter driving course is required to determine the road load than the conventional coastdown test.

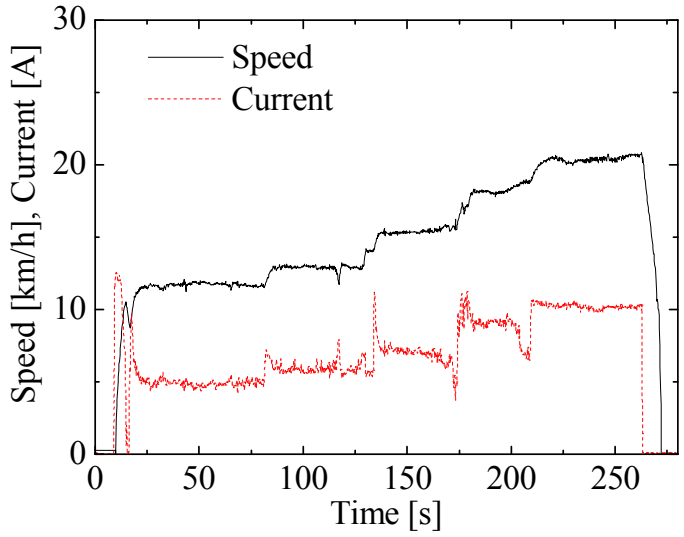

Fig 2.10 Time-speed and battery output current profiles obtained during new method on road.

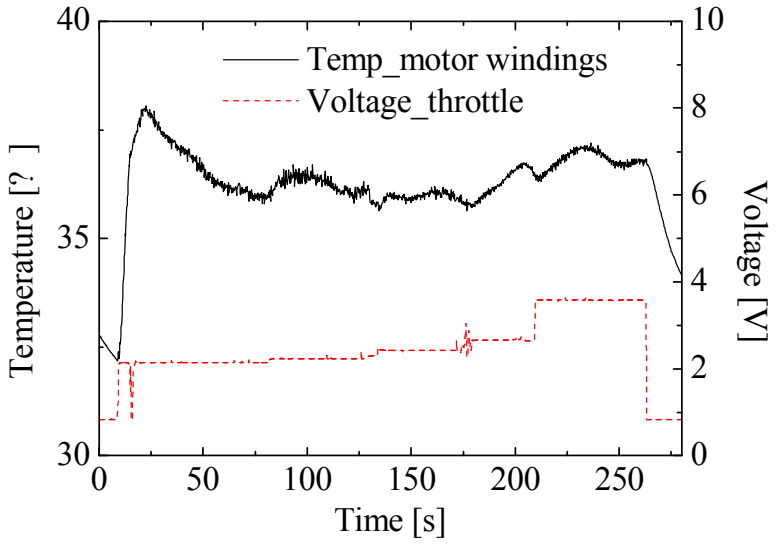

Fig 2.11 Time-temperature of motor winding and throttle output voltage profiles obtained during new method on road.

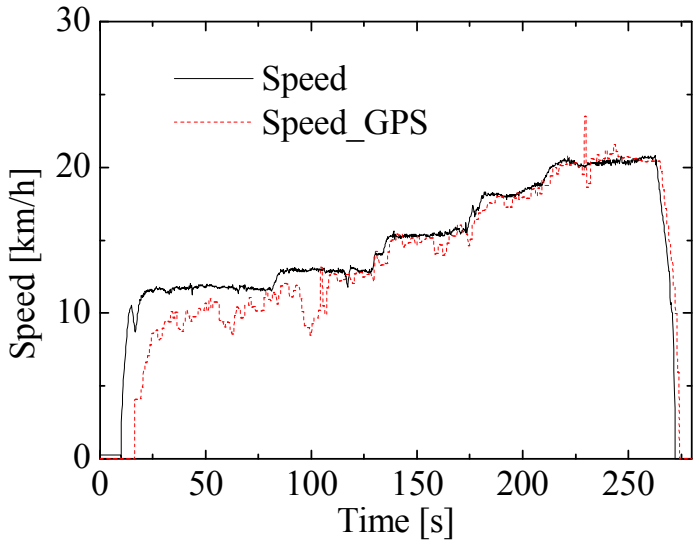

Fig 2.12 Time-speed profiles obtained from the wheel's rotational speed and GPS signals.

2.5 Comparison of the test results between the coastdown test and new method

In the real road test to which the new method is applied, sections with a constant speed of more than 10 seconds are investigated. Figure 2.13 and Figure 2.14 show the time-speed, and time-battery output current graph respectively. The section with a constant speed includes (45–55, 90-100, 141-151, 183-193, 218-228) seconds, and the average value of the speed and battery output current in this section (11.85, 12.95, 15.30, 18.10, 20.36) km/h, and (4.74, 5.87, 7.23, 9.11, 10.28) A, respectively. And the standard deviation of the speed and battery output current is (0.07, 0.07, 0.08, 0.09, 0.15) km/h, and (0.15, 0.19, 0.20, 0.20, 0.13) A, respectively. We derived the following speed-road load correlation equation by substituting the average value of the speed and battery output current in equation (2.7), (2.8) and interpolating it with the least squares method.

$$T_{d,\,sat} = 0.8069 + 0.00005v + 0.0209v^2 \qquad (2.10)$$

$$T_{d,\,nsat} = 0.6663 + 0.00005v + 0.021v^2 \qquad (2.11)$$

As in Fig 2.11 the motor winding's temperature varied by more than

saturation state, the e-bike's motor was considered to be in non-saturation state over the real road test. So equation (2.11) is more adequate for determination of road load than equation (2.10).

Figure 2.15 shows the speed-road load correlation equation obtained through the coastdown test and new method. As shown in Fig 2.15, the road load determined through the new method is less than that obtained through the coastdown test. The errors between the equation (2.11) obtained through the new method and the road load at the 10 reference speeds obtained through the coastdown test are shown in Fig 2.16. Errors of 1.01 Nm, and 1.02 Nm occur at the reference speeds of 4 km/h and 6 km/h respectively, and a small error of less than 1 Nm occurs at other speeds.

In the field test to determine the road load, there are a variety of measurement uncertainty factors that can cause errors. These measurement uncertainty factors include weather conditions, vehicle conditions, driver's driving conditions and measurement errors of the measuring devices. [29, 30] In consideration of the measurement uncertainty factors, it can be inferred from the fact the error of about less than 1 Nm occurred that the road load determined through the new method is highly reasonable.

And if the new method will be applied to determine the road load, the distance of the driving track for the test can be reasonably short compared

to the coastdown test. The new method need the driving track to have a minimum distance to cruise constantly at maximum reference speed for more than 10 seconds, In coastdown test, the e-bike was ridden 97 m from 24 km/h to standstill. But in new method the e-bike just needs about 60 m driving track to cruise constantly at maximum reference speed, 22 km/h for 10 seconds. Therefore, the new method has an advantage that the road load can be acquired in shorter driving track than the coastdown test.

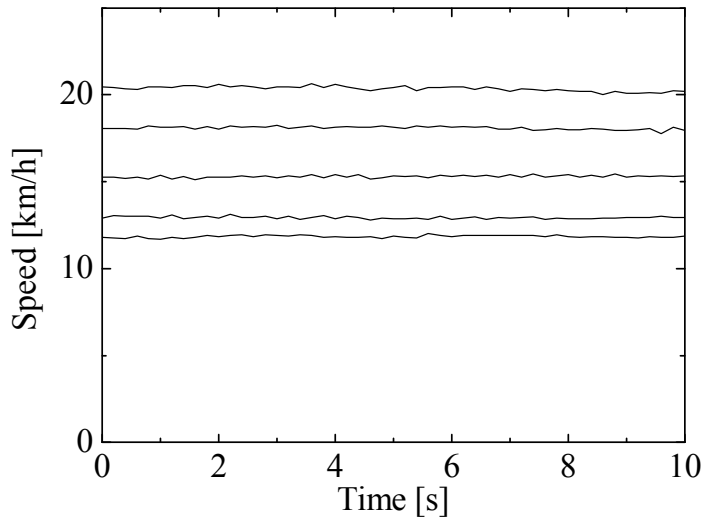

Fig 2.13 Speed variation of e-bike running at constant speed with time in field test.

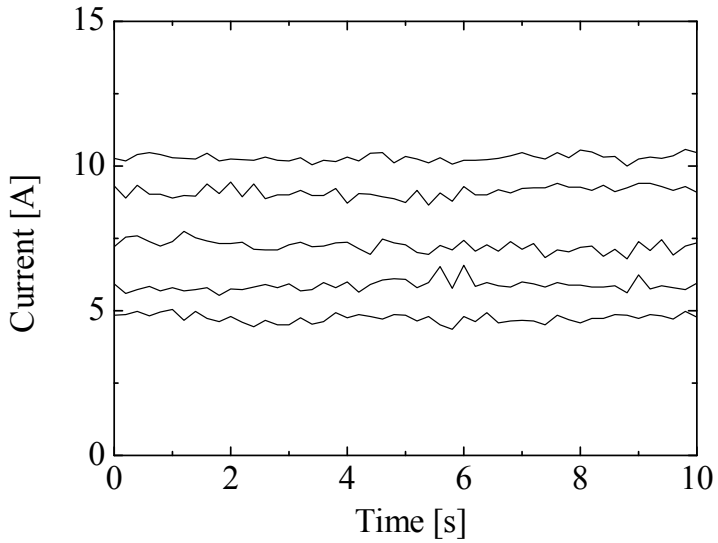

Fig 2.14 Current variation of e-bike running at constant speed with time in field test.

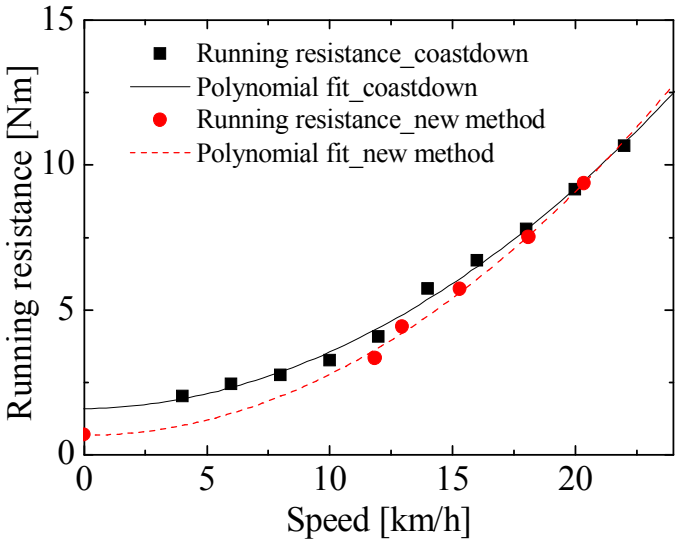

Fig 2.15 Comparison of the correlations between the road load and speed obtained new method and the coastdown test.

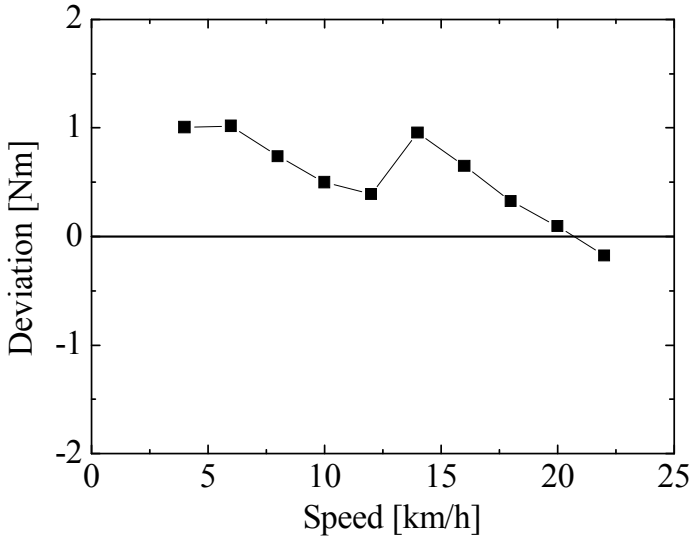

Fig 2.16 Deviation of road loads of coastdown test from ones of new method field test.

2.6 Summary

We developed a new method to determine the road load acting on an e-bike driven by in-wheel BLDC motor, different from the conventional coastdown test. And this method was conducted by measuring the current consumption of the motor and using a correlation of the motor's torque and current when the e-bike is being driven at constant speed. Through the field test, we found that the e-bike motor's current consumption at constant speed could be used to derive the motor's output. After conducting field test for new method, we obtained the second-order polynomial curve for speed and road load, from which the coefficients of rolling resistance, C_0, C_1, and the coefficient of aerodynamic resistance, C_D, were derived.

The new method was verified through comparison with the coastdown test. The road load determined through the new method turned out to be slightly smaller compared to that obtained by the coastdown test. However, the maximum error between the road load obtained from the coastdown and that obtained through the new load was 1.02 Nm, and a small error of less than 1 Nm occurred in most sections. Thus, it can be safely said that this error represents an acceptable value, given a variety of measurement uncertainties that can occur in the real road test.

In conclusion, this method proposed in this study is expected to be

acceptable for determining the road load for e-bike of which the wheel drive electric motor possesses the linearity between torque and current.

Chapter 3. HILS under torque control mode on motor dynamometer combined with the powder brake

3.1 Introduction

In the development stage of a new model, a performance evaluation conducted after mounting the drive module on an electric two-wheeler may burden the drive module manufacturer with significant expenditures of time and financial and human resources, even though it is easier to mount a drive module on this type of vehicle than on a typical passenger car, However, if the motor dynamometers that most manufacturers possess as basic test equipment and the HILS method used in this study are applied to the pre-evaluation of the drive module, these burdens can be reduced significantly. A dynamic simulation of riding the e-bike on a real road was performed on motor dynamometer equipped with the powder brake. The real parts of the e-bike used for the dynamic simulation were the motor, MCU, battery, and throttle device for acceleration. In the case of using a secondary cell such as a lithium-ion battery and fuel cell, the drop in voltage increases with an increase in current in the secondary cell, owing to the increase in internal loss such as

ohmic loss [44]. In other words, during the field test and dynamic simulation, the output voltage of the battery does not remain constant with a variation in the battery current. If DC power supply is used instead of the battery in the dynamic simulation, its supply's voltage must be controlled to simulate the variation in the real battery's voltage [45, 46]. In the dynamic simulation, we adopted to use an identical battery to the one we used in the field test as the power source. We inserted this battery into the simulation loop instead of the numerical equation for the battery, making possible to eliminate the effort of making a numerical model of the battery. And in order to remove the effect of different initial state of charge of the battery during the dynamic simulation, we matched up the open circuit voltage (OCV) of the battery with the one of the battery we used in the field test so that the charging capacities of the battery accorded with each other. We assumed the charging capacity of the battery is mainly related with the OCV of the battery [47].

3.2 Experimental setup

3.2.1 Test setup for field test

On a real road, we conducted the field test riding the e-bike for the coastdown test and the random speed profile test. The field test was carried out at the calm, windless day on an even (nearly zero slope) asphalt road. The

acquired data in the field test were the rotational speed of the wheel, voltage and current of the battery output terminal.

HBM's e-DAQ was used as the data acquisition system (DAQ) of the field test, and LEM's HAIS 50-P was used as current sensor. We read the output voltage of the battery through the analogue input channel of e-DAQ directly. Figure 3.1 shows the experimental set up for the field tests.

The wheel's rotation speed was measured by two methods. One method involved calculation of the rotation speed from the frequency of the digital pulse output of the hall sensor mounted on the stator, which was measured using the digital counter channel of the e-DAQ. The results of a waveform analysis of the hall sensor revealed that its digital pulse was generated 44 times per rotation. The e-bike's speed was derived from the hall sensor's frequency, the pulse per rotation, and the wheel radius. The Output pulse of the hall sensor inside the BLDC motor during one rotation is shown at Fig 3.2.

The other method of determining the wheel's rotation speed involved counting the pulses from the electric circuit, which consisted of a pull-down resistor and a reed switch. The reed switch, obtained from a commercial speed meter for bicycles, is normally open and closes when a magnet installed on a spoke of the wheel is present. The pulse outputs per rotation were also measured through the e-DAQ.

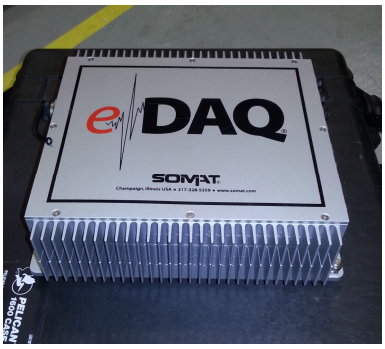

a) e-DAQ

b) Current sensor

c) picture of field test of e-bike

Fig 3.1 Experimental set up in field test.

After the wheel rotation speed data obtained by the two methods were calibrated, the speeds obtained were confirmed to be the same.

The test e-bike was equipped with the in-wheel motor and Li ion battery. The inner structure of the drive motor is shown in Fig 3.3 which gives the details of rotor, stator, hall sensors and differential gears. The detailed specification is shown in Table 3.1.

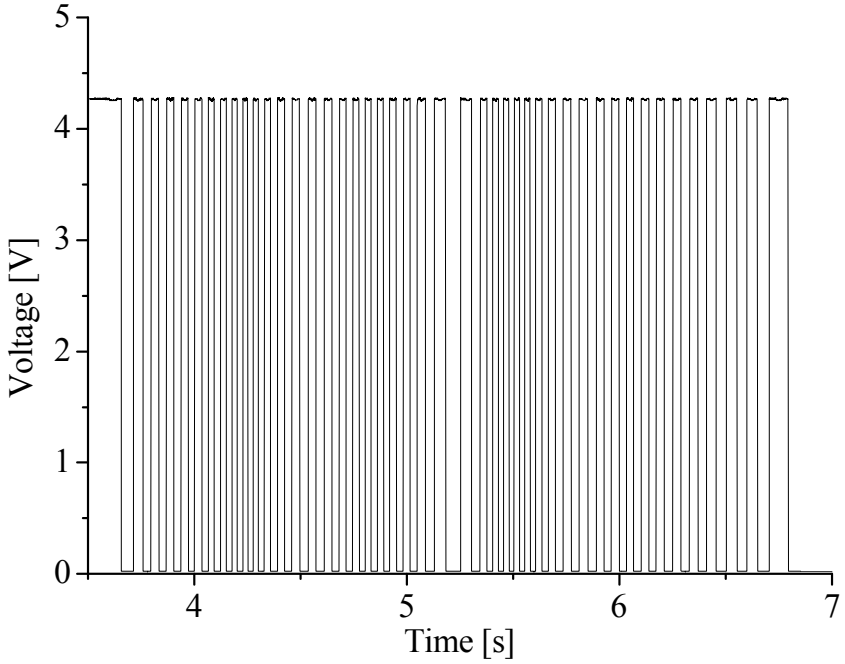

Fig 3.2 Output pulse of the hall sensor inside the BLDC motor.

a) Inner structure of the drive motor containing rotor, stator, and hall sensors

b) Differential gears of the driver motor

Fig 3.3 Structure of the drive motor.

Table 3.1 Specifications of e-bike, battery and test motor.

Parameter	Value	Unit
E-bike		
Weight	19.15	kg
Wheel radius	24.25	cm
Rider weight	84.00	kg
Mobile DAQ weight	7.36	kg
Regenerative braking mode	No	-
		-
Battery		-
Type of battery	Lithium ion	-
Nominal voltage	36	V
Nominal capacity	7.2	Ah
Test motor		
Type	Brushless DC motor	-
Rotating part	Outer rotor	-
Rated output	250	W
Rated voltage	36	V
Rated rotating speed	220	rpm
Rotating speed at no load	280	rpm

3.2.2 Dynamic simulator

The hardware configurations for dynamic simulator are identical to the ones of the dynamometer for the motor characteristic tests mentioned in previous chapter 2. But the software configurations significantly change in this dynamic simulation process. The software based on labview for the motor characteristic tests is replaced with the one which has the road load model for the e-bike and the two PI controllers for the speed control applied at throttle device and the torque control applied at the powder brake.

3.2.3 Calibration of the measurements from motor dynamometer test and field test

In the motor characteristic test, the motor current consumption, battery output voltage, and motor rotating speed were simultaneously measured using the mobile DAQ used in the field test. The compared values were calibrated in the mobile DAQ against those used in the software program with the motor dynamometer. Using these calibrations, we could compare the field and dynamic simulation test results accurately and consistently.

Figure 3.4 and Figure 3.5 show the deviation of rpm and current respectively, which are the values subtracted measured data in the software program with the motor dynamometer from those using the mobile DAQ.

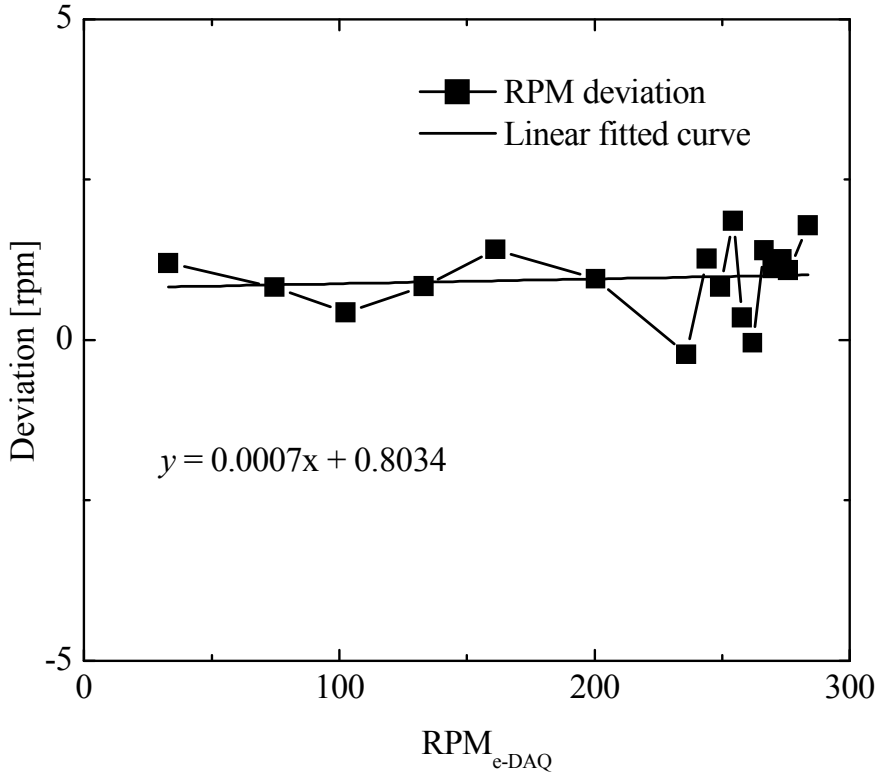

Fig 3.4 Deviation of rpm measured in DAQs used in the motor dynamometer and the field tests

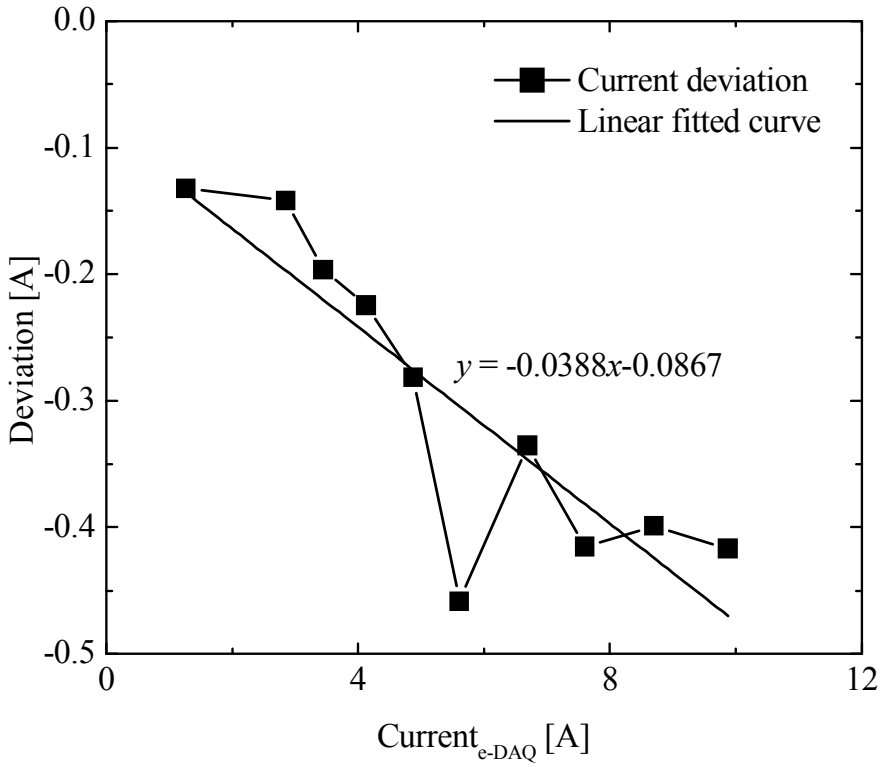

Fig 3.5 Deviation of currents measured in DAQs used in the motor dynamometer and the field tests

3.3 Coastdown test

The coastdown test procedure involves accelerating the vehicle to as high a speed as practicable, disengaging the transmission, setting the gear position to neutral, and allowing the vehicle to coast to a low speed without any drive power. The time–speed profile is obtained by simultaneously recording the time and vehicle speed, and using this profile, the relation among speed, rolling resistance, and aerodynamic resistance is determined.

During driving, the vehicle is subjected to a road load, which consists of running and inertial resistances. The total running resistance consists of rolling, aerodynamic, and grade resistance, as shown in equation (2.1) of chapter 2.

The time–speed profile shown in Fig 3.6 was obtained from the results of the coastdown test. The road loads corresponding to the six reference speeds (10, 12, 14, 16, 18, and 20 km/h) were obtained using equation (3.1).

$$T_{d,\,ref} = rF_{d,\,ref} = rm_a((v_{ref} + \Delta v) - (v_{ref} - \Delta v)) / \Delta t = 2rm_a \Delta v / \Delta t \qquad (3.1)$$

The value of Δv in equation (3.1) was set to 2 km/h, and the value of Δt, which is the time interval from $v_{ref} + \Delta v$ to $v_{ref} - \Delta v$, was calculated from the time–speed profile obtained from the coastdown test results. The speed–road

load data obtained are shown in Fig 3.7. The data were fitted approximately to the second-order polynomial curve that is shown in the figure and expressed by equation (3.2), obtained by applying recursive least-squares fitting. As it is unrealistic for the rolling resistance parameters C_0 and C_1 to have negative values, the curve was fitted for positive values. [28]

$$T_d = 1.4215 + 0.00001v + 0.0331v^2 \tag{3.2}$$

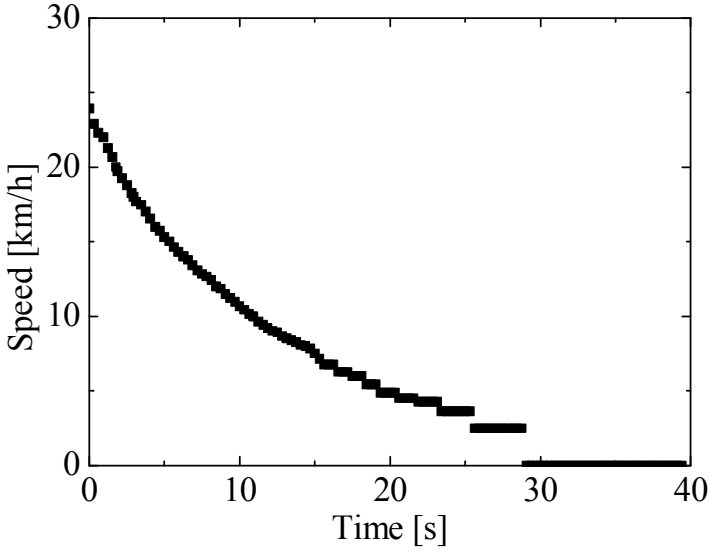

Fig 3.6 Time-speed profile of coastdown test on road

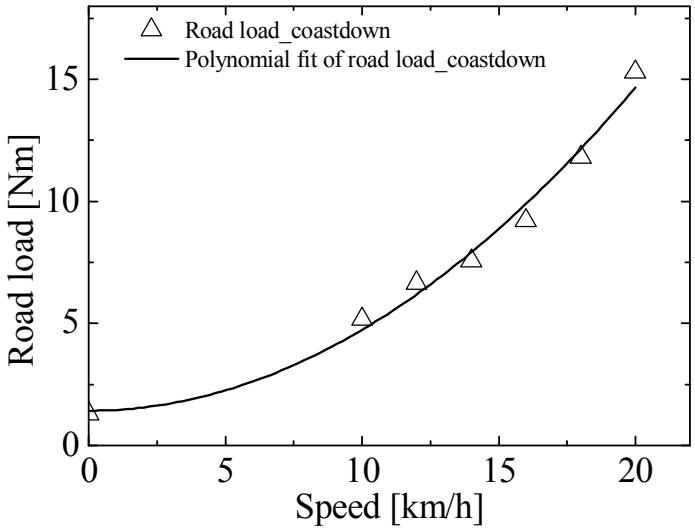

Fig 3.7 Running resistance torque-speed correlation on road

3.4 Dynamic simulation

Figure 3.8 shows the system configuration of the e-bike's dynamic simulation on a motor dynamometer. And Figure 3.9 shows the dynamic simulation procedure. To control the motor's operation so that it precisely follows the time-speed profile obtained from the field test, we used two proportional-integral (PI) controllers for speed and the consequent road load, which were operated independently and sequentially. Substituting the motor speed in equation (3.2), the road load through the powder brake corresponding to the rolling and aerodynamic resistances acting on the motor combined with the inertial resistance resulting from acceleration and deceleration can be determined. The road load equal to T_e, to which the motor on dynamometer is subjected through the powder brake, can be expressed as equation (3.3).

$$T_e = T_d + rm_a\, dv/dt = 1.4215 + 0.00001v + 0.0331v^2 + rm_a\, dv/dt \qquad (3.3)$$

The inertial resistance torque is equal to the apparent mass of vehicle times the wheel radius and acceleration, speed variation per time variation. In our study, we assumed the apparent mass of the e-bike is equal to the total mass of e-bike multiplied by 1.03 considering the equivalent mass of the rotating parts as the 3 % of the total mass of e-bike.[3, 39] Acceleration was

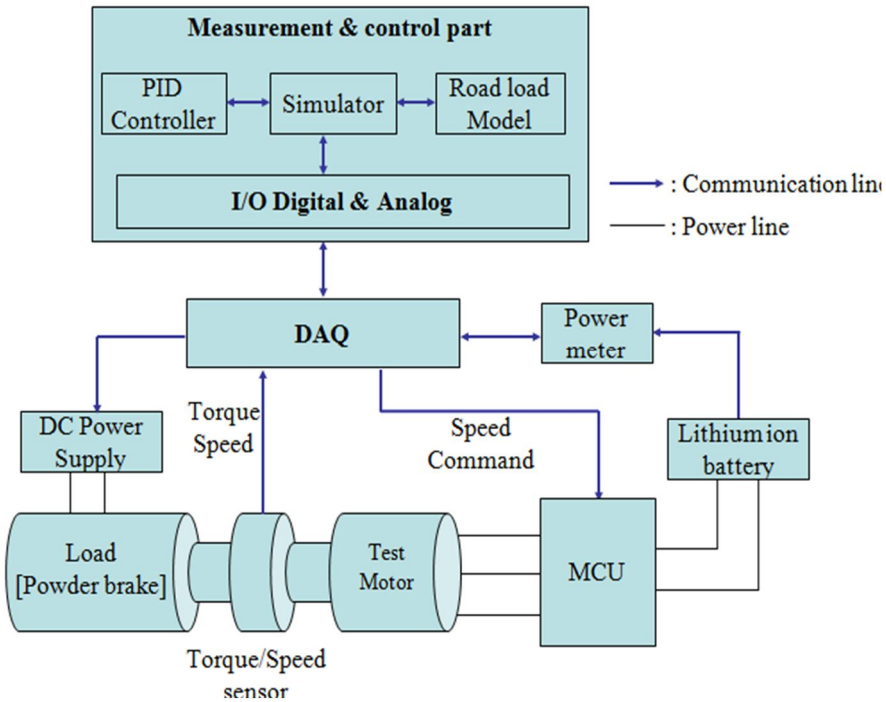

Fig 3.8 System configuration of e-bike's dynamic simulation on motor dynamometer

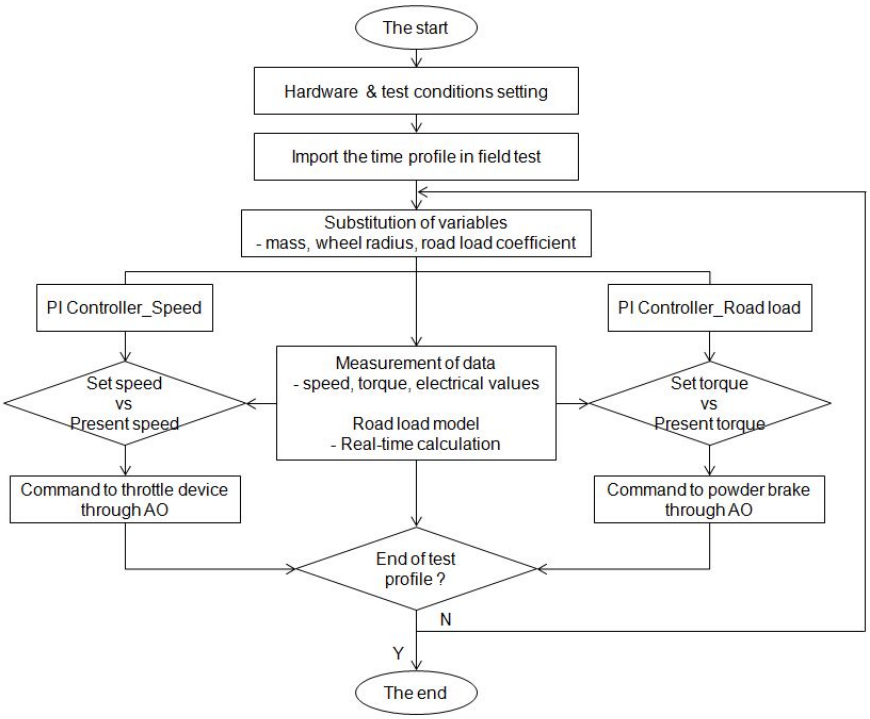

Fig 3.9 Dynamic simulation procedure with the powder brake operated at torque control mode

obtained from the measurement of the speed variation during specific time intervals. In dynamic simulation, the iteration period was kept to 50 ms, while the control of speed and road load was made, simultaneously measuring the data and calculating the road load. Because there are uncertainties and ripple of speed data if the time interval for calculation of acceleration is 50 ms, we decided acceleration was determined by measurement of the speed variation during one second. After measuring the data and calculating the road load in the iteration loop, road load was applied to motor through powder brake which was controlled by P-I controller in the form of friction force.

The loader on a motor dynamometer that simulates the road load on a vehicle can operate in two ways: torque control mode or speed control mode. An active loader, such as a servo motor or M-G set, can operate both in torque control mode and speed control mode, while an inactive loader, such as a powder brake, can operate only in torque control mode. Torque control mode is usually applied to HILS when the time–speed schedule is predefined and the vehicle's speed is controlled by the simulator automatically. In this study, the powder brake was operated in torque control mode, and the vehicle's speed was controlled using a PI controller. The powder brake was able to effectively simulate the positive inertial resistance during acceleration from a standstill, even without the flywheel representing the rotating inertia of the e-

bike. To minimize the effect of the absence of the flywheel in the simulation of deceleration in the field test, the e-bike was ridden with power from the motor, without coasting or braking. During the field test, data were measured at a sampling rate of 1.6 samples/s, so the time interval for acceleration was 0.625 s.

The motor's speed is controlled in the range 0–280 rpm using the throttle device in the handgrip, rotating which generates an analog voltage output from 1.4 to 3.5 V. In the dynamic simulation, the analog output channels in PCI-6229 simulated this signal as analog voltage. The powder brake was powered by a related power supply of 0–10 V, and its braking performance was ~0–100 Nm, linearly proportional to the voltage. In the dynamic simulation, the two PI controllers fixed the real-time speed and road load to set points by effecting feedback control of the throttle's output signal and the power supply's input signal for the powder brake, respectively.

3.5 Starting characteristics of the e-bike in the dynamic simulation

Before the dynamic simulation on motor dynamometer about the random driving cycle was carried out, the starting characteristics of the e-bike's drive motor was investigated on motor dynamometer when the inertial resistances

due to the sudden acceleration increased overwhelmingly. The objective of this simulation was the verification of the fast response of the powder brake against to the input set-command, the set road load containing the increasingly inertial resistance. The e-bike's drive motor was equipped on the motor dynamometer and accelerated for about 10 seconds by rotating the throttle device suddenly. The coefficients for road load were selected randomly and they were 1.5, 0.0002 and 0.04 for C_0 and linear $C_r(v)$, respectively, considering the e-bike's weight and driver motor's characteristics. Figure 3.10 and 3.11 show the time profile of the speed, current and voltage and the time profile of the real/set road load on motor dynamometer, respectively. At starting points, about 3 seconds later, the in-rush currents flew into the motor abruptly and then the voltage drop of the battery occurred since the inertial resistance increased in a moment. And the response of the powder brake against the set road load was seen to be delayed about 1 second later as shown in fig 3.11. The road load of the e-bike during the riding was considerably variable and the main reason was that the variation of the speed was continuously produced and made the inertial resistance of the total resistances variable continuously. At fig 3.11, it was seen that the set road load was also variable along to the speed variation, but the real road load implemented by the powder brake was somewhat smooth comparing the set road load. It was

assumed that the powder brake's response couldn't keep up to the input command for the set road load. And at next chapter, these response characteristics were considerably improved by adopting the servo motor instead of the powder brake on motor dynamometer.

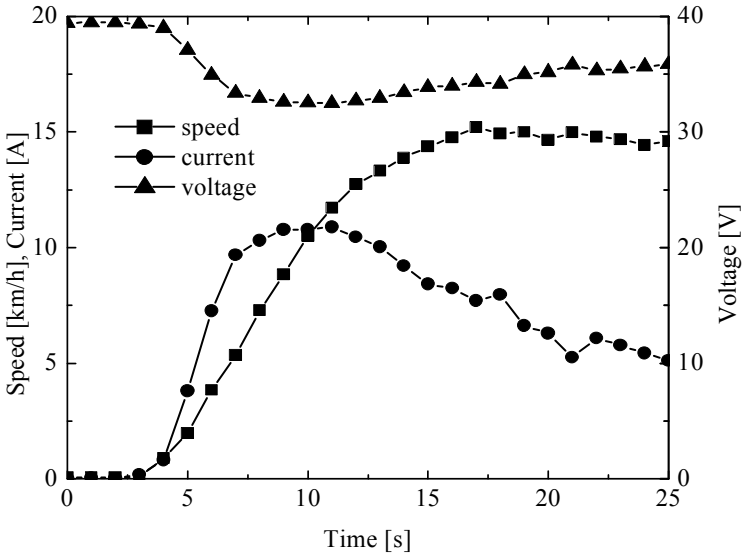

Fig 3.10 Speed, current and voltage profiles of the drive motor of the e-bike at starting from standstill in dynamic simulation.

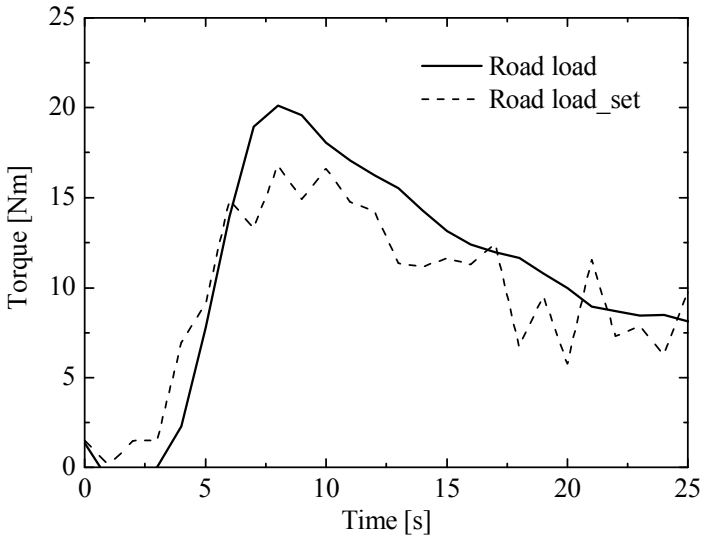

Fig 3.11 Real/Set road load profiles of the drive motor of the e-bike at starting from standstill in dynamic simulation.

3.6 Comparative analysis of simulation and field test

The results of the field test and dynamic simulation are shown in Fig 3.12–16 in terms of the speed, road load, voltage/current, power, and input energy, respectively. Figure 3.12 shows the time-speed profiles of the field test using the mobile DAQ and in the dynamic simulation on the motor dynamometer. There is no standard driving cycle for the e-bike's driving performance, unlike for the IC engine vehicle, which has standard city driving (FTP-75) and highway driving (HWFET) cycles. Hence, we rode the e-bike for about 150 s according to an arbitrary driving cycle considering the short driving distance on a real road, less than 600 m. In the field test, we did not brake except for a stop at 135 s and observed that rapid changes in voltage, current, and power like step responses occurred during the acceleration period corresponding to 15 s, 35 s, and 49 s, and during the deceleration period corresponding to 81 s, 95 s and 129 s. We assumed that the above phenomena occurred due to the inrush or sudden stop in the current flowing into the motor when the throttle device in the handgrip was instantaneously rotated for acceleration or deceleration. The time-speed profile obtained through the dynamic simulation using the method described in section 3.4 was plotted along with that obtained from the field test.

Figure 3.13 shows the time-road load profiles in field test and dynamic

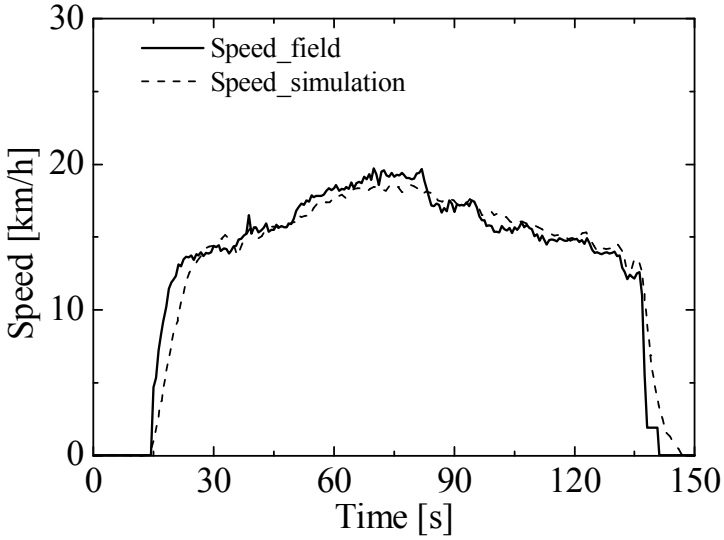

Fig 3.12 Speed tracking performance of dynamic simulation on motor dynamometer

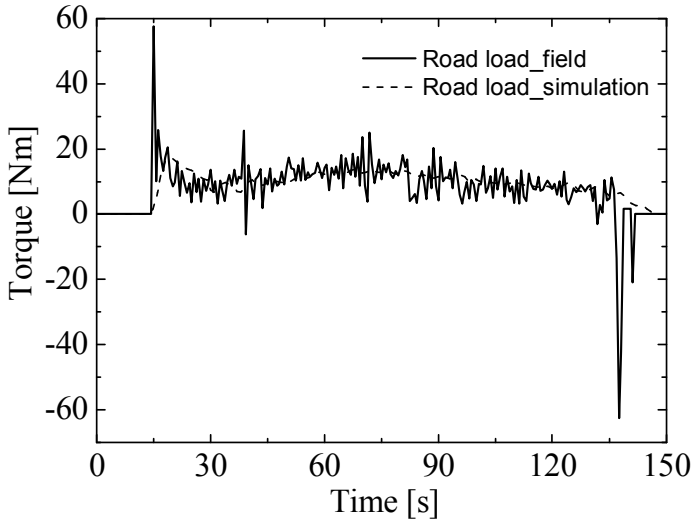

(a) Road load in field test and dynamic simulation

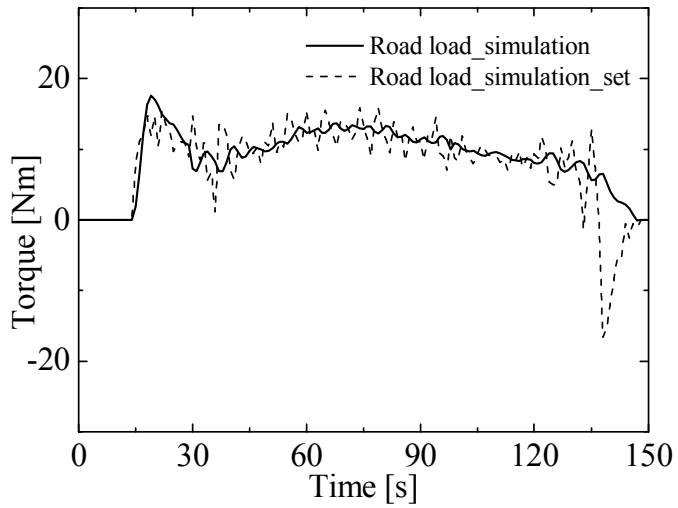

(b) Set value and actual value of road load in dynamic simulation

Fig 3.13 Road load profiles in field test and dynamic simulation

simulation. In Fig 3.13-a), the road loads in the field test and the dynamic simulation to which the drive motors of the e-bike were subjected to were plotted together. The road load in the field test was calculated from equation (5) by substituting the vehicle speed and the acceleration. The acceleration was derived from the vehicle speed variation during the sampling time, which was 0.625 s. Especially at the starting time, the amount of road load in the field test is considerably greater due to the immediate increase of inertial resistance. In the case of the dynamic simulation, because the powder brake didn't start to operate locking the drive motor at the starting time, the amount of road load at the starting time in the dynamic simulation is lesser than the one in the field test. Because of the MCU's function to limit the over current into motor, the input current was not increased proportional to the output torque from about 12.1 A. And in Fig 3.13-b), the set road load through the P-I controller and the resulting real road load subjected to the motor was plotted. From Fig 3.13-b) we found the physical response of the powder brake toward input signal was late. It seems that the powder brake has, to some extent, a response delay to the input signal. But if we shorten the iteration period for control, 50 ms, we think this response delay will be improved.

Figure 3.14 shows the variation in the battery output voltage and input current into the MCU with time for both tests. As the e-bike's speed increased,

we found that the current consumption of the motor increased because of the increase in the running resistance. At starting and at acceleration, inrush current flowed into the motor owing to an increase in the inertial resistance and small back-electromotive force. When the throttle device was quickly released at 81, 95 and 129 seconds in field test, the current into the motor suddenly stopped owing to the MCU's response to the output signal from throttle. However, these phenomena were not observed in the dynamic simulation, because the PI controller made the speed of the motor follow a set point, which was the speed profile in field test, not the output voltage of the throttle device. While the sudden stop of the current into motor and the instantaneous increase of the battery voltage occurred during the quick release of the throttle, the speed of the motor didn't decrease as rapidly like the output voltage of the throttle device.

Figure 3.15 shows the variation in the motor power consumption with time during both tests. Since the power consumption of the motor is the battery output voltage times the MCU current consumption, the time-power profile is very similar to the time-current profile. As shown in Fig 3.16, the input energy into the motor in the field test steadily increased owing to the absence of a rest period, and is slightly more than that in the dynamic simulation. The difference, about 0.6 Wh or 2.2 kJ, was considered the result

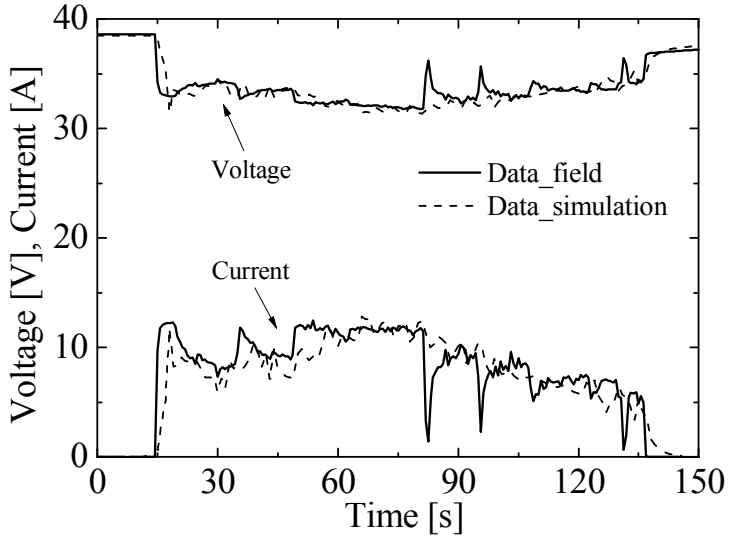

Fig 3.14 Voltage/current tracking performance of dynamic simulation on motor dynamometer

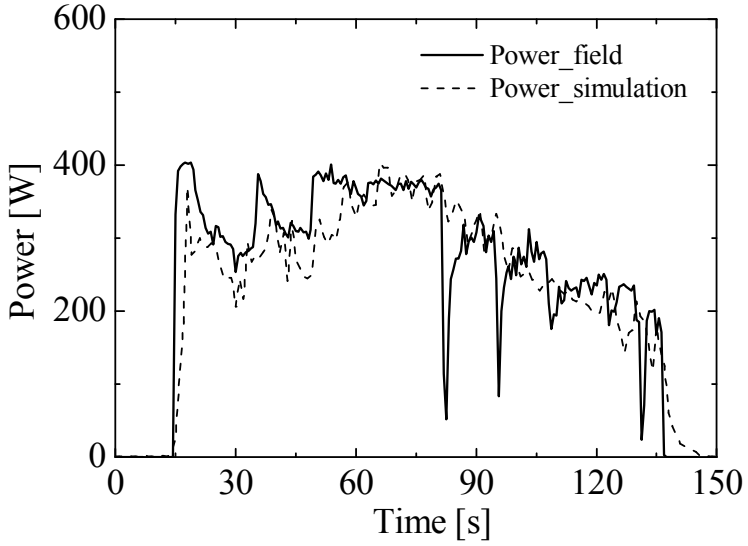

Fig 3.15 Power tracking performance of dynamic simulation on motor dynamometer

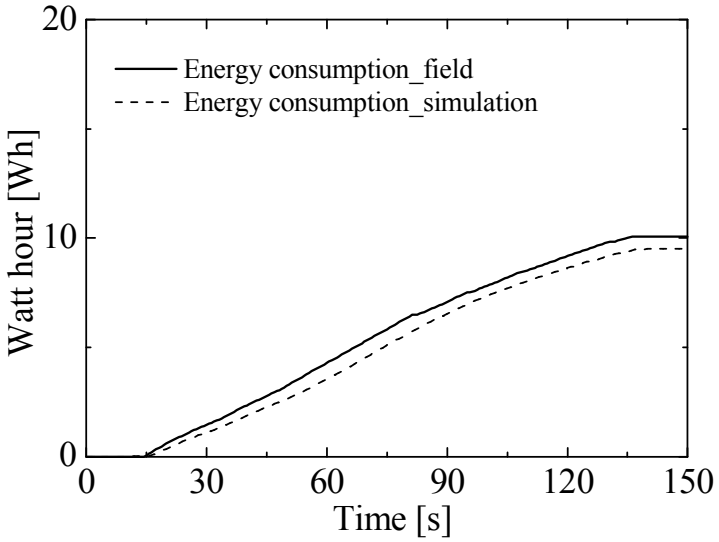

Fig 3.16 Energy consumption tracking performance of dynamic simulation on motor dynamometer.

of the current deviation caused during acceleration and deceleration.

The differences between the simulation results and field test data for speed, voltage/current, and power/energy are shown in Fig 3.17, 3.18, and 3.19, respectively. Table 3.2 shows the deviations of the simulation results from field test data and energy efficiencies. It can be seen that the speed in the dynamic simulation satisfactorily follows the time-speed profile of the field test. The average and standard deviations of tracking errors are 0.04 km/h and 1.18 km/h, respectively, except during the starting (about 15 s) and ending (140 s) periods. During the dynamic simulation of the acceleration and deceleration of the field test, a time delay in simulated speed from the actual speed in the field test was generated, because the PI controller could not receive the feedback command for the motor's speed in real time. If we later adopt the dynamic simulation procedure for real-time operations (HILS), this time delay will be considerably reduced. In the case of approximately constant speed sections (70–80 s and 110–120 s), the tracking performance in the dynamic simulation was satisfactory.

The average and standard deviations of tracking errors for current were 0.11 and 0.48 A, respectively, for 70–80 s, and -0.36 and 0.70 A, respectively, for 110–120 s. This means that the road load determined by our proposed method very well represents the running resistance. If we integrate speed and

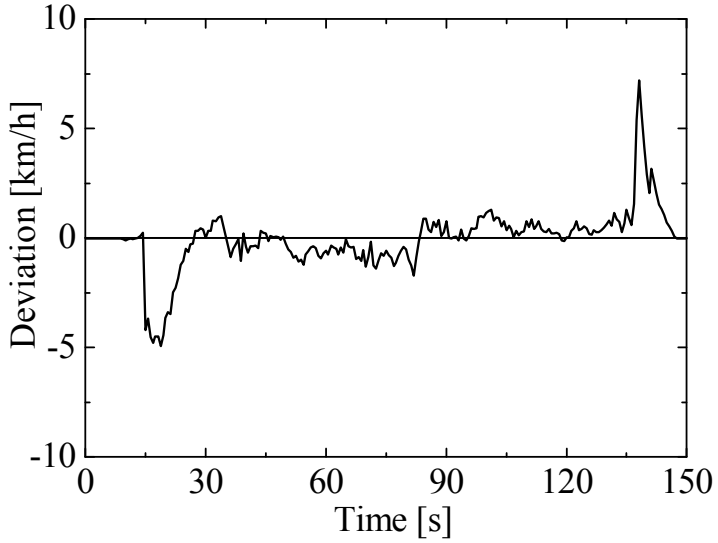

Fig 3.17 Deviation of speed in dynamic simulation from field test results.

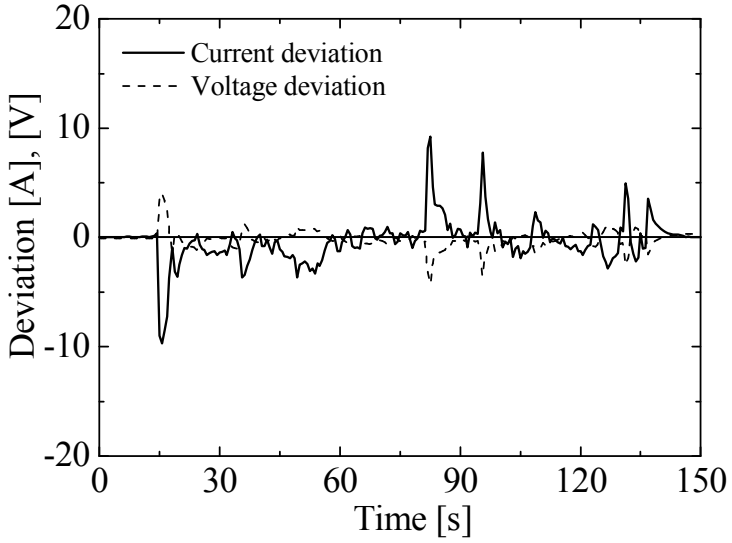

Fig 3.18 Deviation of voltage/current in dynamic simulation from field test results

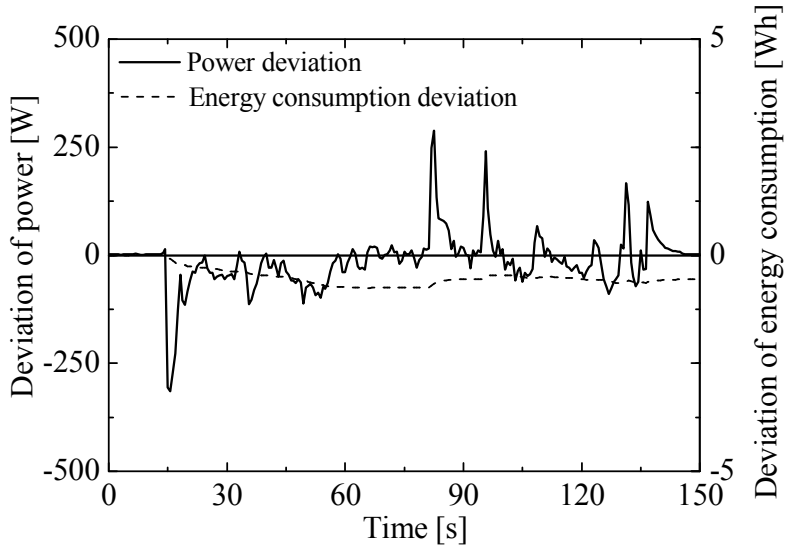

Fig 3.19 Deviation of power/energy consumption in dynamic simulation from field test results.

Table 3.2 Deviation of the simulation results from field test data and energy efficiencies.

1) Deviation of the simulation results from field test data			
	Average	**Standard deviation**	
Speed [km/h]	0.04	1.18	Except during starting (15 s) and ending (140 s) periods
Current [A]	0.11	0.48	For 70–80 s
	-0.36	0.70	For 110–120 s
2) Energy efficiency			
	Field test	**Simulation**	
Total drive distance [m]	538	535	
Consumed energy [Wh (kJ)]	10.08 (36.29)	9.52 (34.27)	
Energy efficiency [Wh/km]	18.7	17.8	

power in a short time interval, we can obtain the drive distance and the energy consumed, respectively. The total drive distance and the consumed energy were 538 m and 10.08 Wh (36.29 kJ), respectively, for the field test and 535 m and 9.52 Wh (34.27 kJ), respectively, for the dynamic simulation. Therefore, the energy efficiencies in the field test and dynamic simulation are 18.7 and 17.8 Wh/km, respectively. Fig 3.20 shows the variation in the fuel efficiencies in the dynamic simulation and field test results over time. These results are considered acceptable if rapid acceleration and deceleration are taken into consideration.

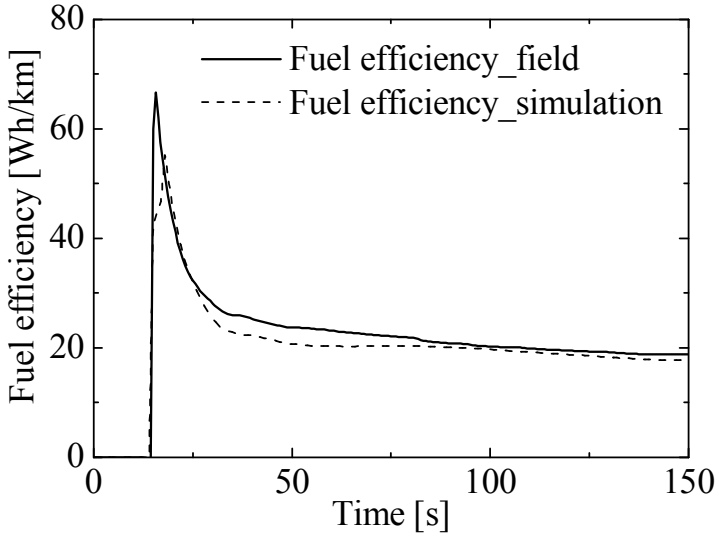

Fig 3.20 Fuel efficiency variation in dynamic simulation and field test

3.7 Summary

A dynamic simulation method on motor dynamometer, HILS in mechanical level was studied to evaluate the drive performance of an e-bike driven by an electric motor, different from the existing chassis dynamometer test. From the quantitative analysis of the drive performance between the dynamic simulation and the field test, we found the dynamic simulation method on motor dynamometer could be very available for the drive performance evaluation of the complete e-bikes only with the drive motor and battery.

Though there was a time delay in the speed, voltage, and current during acceleration and deceleration in the dynamic simulation, this was mainly due to the delay in the response to the feedback command of the PI controller. When the e-bike's speed reached a rather constant value, we noticed that the motor was being subjected to the same road load as that when riding on a real road.

In conclusion, this dynamic simulation method is considered to be acceptable for an effective means of pre-evaluation of the drive motor or battery prior to the production of complete vehicles. And we expect more extensive and detailed studies on this method will be conducted for various EVs, including e-bikes.

Chapter 4. HILS under speed control mode on motor dynamometer combined with the servo motor

4.1 Introduction

In respect of the evaluation of the performance and reliability of the developed products, it is one of the essential parts to reproduce the real operating condition of the test products. HIL (hardware in the loop) test is a wide-used test technique to reproduce the real operating condition in laboratory space, not in a real operating place. In testing the drive performance of a vehicle, HIL tests can be effectively applied. The drive performance test of the vehicles through the chassis dynamometer also can be considered to be one of the HIL tests, because this test makes the laboratory test of the vehicle drive performance possible by applying the road load to the test vehicle on chassis dynamometer, not real road.

In this study, we have developed a dynamic simulator for the drive performance test of the electric two-wheelers which simulates its drive on a real road using the motor dynamometer combined with the servo motor, not the chassis dynamometer. Prior to our study, many studies about HIL tests in

the field of the automotive engineering were carried out. He et al. *[18]* put forward a fuzzy logic-based control system of hybrid power/energy used in electric vehicles and evaluated the performance of the proposed control system using HIL test. Ahlawat et al.[48] studied the development of engine and vehicle models for performing HIL tests on automotive transmissions. Through the HIL test setup, they could perform the laboratory test to subject the transmission to in-vehicle transients, capturing all the dynamics of interest. Petersheim et al. [49] investigated the dimensionless formulation using HIL simulation to scale the signals in and out of the prototype system like electric motor and battery of the electric vehicle in order to represent production-sized components. Their dimensionless formulation was used to rescale prototype vehicle power train component models to emulate full-scale counterparts. Kim et al. [50] performed a HIL validation of their developed power management strategy, with a real engine and battery integrated into a diesel hybrid electric vehicle simulation. They developed a networked HIL simulation platform for their strategy validation, to enable a system integration despite the fact that the components resided in different geographic locations. Their networked HIL simulation platform was developed so that the sensitivity of the simulation to communication delays between the locations of the coupling point was minimized.

Especially, studies about HIL tests in the field of the vehicle's engine (or motor of electric vehicles) dynamometer was carried out in the purpose of the performance and reliability test of the vehicles and their parts. Babbitt et al. [51] had developed the HIL virtual engine loading system for use in engine and power train research, as well as control and diagnostic algorithm development and validation. But in their dynamometer engine test system, the inertial load of the road load was not implemented because of the lack of the control technique like the high-resolution acceleration estimates and precise torque control. Fajri et al. [52], Zha et al. [53] and Li et al. [54] investigated the approaches of electric vehicle (EV) drive emulation on a test bench setup consisting of a drive motor connected to a dynamometer. In their studies, the load motor on the dynamometer connected to a drive motor implemented the road load occurred during the drive. And their studies on the EVs mainly focused on the drive performance characteristics of the drive motor not including the battery's performance like discharging performance. In the case of the electric two-wheelers, especially e-bikes whose battery output voltage can be varied according to the transient load variation, the drive motor of the e-bikes is subjected to an inevitable speed change according to the variation of the battery output voltage.

In this study, we have developed the dynamic simulator which

implemented the HIL test for the drive performance evaluation including the drive motor and the battery of the e-bikes as the real hardware inserted in the simulation loop. Through this dynamic simulator, we could simulate the transient mechanical load the drive motor experienced and investigate the torque characteristics of the drive motor and the discharging performance of the battery during the drive. In the dynamic simulator, the load machine, the servo motor of the motor dynamometer applies the road load to the motor under test according to its speed and the acceleration. And the road load which the servo motor applies to the drive motor consists of the running resistance and the inertial resistance represented by a function of the speed and the acceleration of the vehicle, respectively. It is known that the running resistance is fitted to the polynomial function, generally second order of the vehicle's speed and the correlation between the running resistance and the vehicle's speed can be derived from the coastdown test in a real road. [27, 28] We carried out the coastdown test by riding the e-bike on the real road, and then acquired the correlation between the running resistance and the vehicle's speed. The inertial resistance is applied by the load servo motor of the motor dynamometer which was controlled by the internal controller inside the driver of the servo motor.

When the servo motor is applied in the HIL test of the vehicle dynamics,

it has conventionally two kinds of the operating mode, torque control mode and speed control mode according to the control subjects of the internal motor driver. In the torque control mode of the servo motor, the test motor is usually controlled to operate according to the predefined driving cycles and simultaneously the servo motor applies the road load calculated from the speed and the acceleration to the test motor. On the other hand, in the speed control mode of the servo motor, the test motor is supposed to operate in accordance with the servo motor's speed which is derived from the speed and the acceleration of the test motor. Also in the speed control mode of the servo motor, the test motor can operate randomly regardless of the predefined driving cycles like FTP (Federal Test Procedure)-75 mode. In order to implement the random driving cycle like the coastdown drive and max acceleration mode in our proposed dynamic simulator, we operated the servo motor in the speed control mode in this study.

We verified the feasibility of our proposed dynamic simulator by comparing the results of the simulation through the dynamic simulator and the field test of the e-bike on the real road about the acceleration test and the coastdown test. This verification process was carried out to ensure that our dynamic simulator could effectively implement the drive performance test of the electric two wheelers only using the drive motor and the battery without

the preparation of the complete vehicle and the large test equipment like the chassis dynamometer. We expect our proposed dynamic simulator will eliminate several constraints of time, cost, place and so on necessary for the drive performance test of the motor driven EVs and expand the range of the feasible test.

4.2 Experimental set-up

4.2.1 Test set-up for field test

On a real road, we conducted the field test riding the e-bike for the coastdown test and the acceleration test from standstill. Figure 4.1 shows the picture of the test e-bike, and the field test was carried out at the calm, windless day on an even (nearly zero slope) asphalt road. The acquired data in the field test were the rotational speed of the wheel, voltage and current of the battery output terminal.

National Instrument's cRio-9022 was used as the data acquisition system (DAQ) of the field test, and LEM's HAIS 50-P was used as current sensor. We read the output voltage of the battery through the analogue input channel of cRio-9022 directly. The speed of the e-bike was derived from the measured wheel rotation speed and the radius of the wheel and we measured the wheel rotation speed through the pulse output generated from the circuit which is

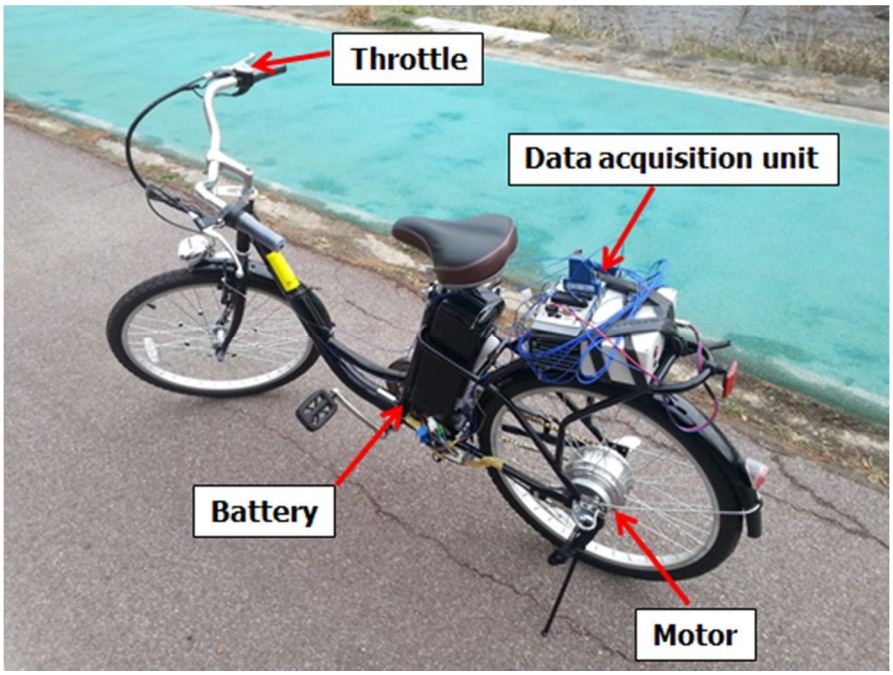

Fig 4.1 Picture of the test e-bike and its comprising parts.

Table 4.1 Specifications of e-bike, battery and test motor.

Parameter	Value	Unit
E-bike		
Weight	30.58	kg
Wheel radius	30.48	cm
Rider weight	84.00	kg
Mobile DAQ weight	3.10	kg
Regenerative braking mode	No	-
		-
Battery		-
Type of battery	Lithium ion	-
Nominal voltage	36	V
Nominal capacity	7.2	Ah
Test motor		
Type	Brushless DC motor	-
Rotating part	Outer rotor	-
Rated output	220	W
Rated voltage	36	V
Rated rotating speed	190	rpm
Rotating speed at no load	240	rpm

comprised of the reed switch and pull down resistor. The reed switch operated as on-off switch according to the presence of the magnets installed in the spokes of the wheel.

The test e-bike was equipped with the in-wheel motor and Li ion battery and the detailed specification was shown in Table 4.1

4.2.2 Dynamic simulator

We set up the dynamic simulator on the motor dynamometer which reproduced the time-speed profiles obtained from the acceleration test and the coastdown test on a real road. The dynamic simulator mainly comprises the load motor, the motor and the battery under test, the DAQ and control parts. The load motor is an asynchronous motor which has the forced air-cooled ventilation and its rated power, torque and speed is 12 kW, 200 Nm and 1000 rpm, respectively. The servo motor used in this study can operate in the manner of the torque control mode and the speed control mode. In the HIL test system about the vehicle's engine dynamometer, the servo motor as the load machine needs to operate in the manner of the torque control mode and the speed control mode based on predefined speed cycle and unpredictable speed profile, respectively.[52] In this study, the servo motor operated in the manner of the speed control mode because in the simulation of the coastdown

and the acceleration, the drive motor during the test rotated according to the correlation between the speed and the road load including the running and inertial resistance, not the predefined time-speed profile. The servo motor has the internal P-I controller for the speed and the torque which conducts the close loop control with approximate 1 ms loop time. This short loop time gives the servo motor a fast response to the input signal, where fast responsiveness means the low inertia of the servo motor.

The drive motor and the battery which had the same specification as ones used in the field test were used in the simulation. National instrument's PCI-6229 was used for data acquisition and control of the load motor and the drive motor under test. ETH's DRFL-Ⅲ was used as torque and speed sensor with an uncertainty of ± 0.2 Nm and ± 1 rpm, respectively. And LEM's HAIS 50-P was used for current sensor with an uncertainty of ± 0.5 A. Figure 4.2 shows the picture of the dynamic simulator on the motor dynamometer.

4.3 Field test

4.3.1 Coastdown test

The running resistance can be calculated from the time-speed profile of the coastdown test on an even road. We carried out the coastdown test by

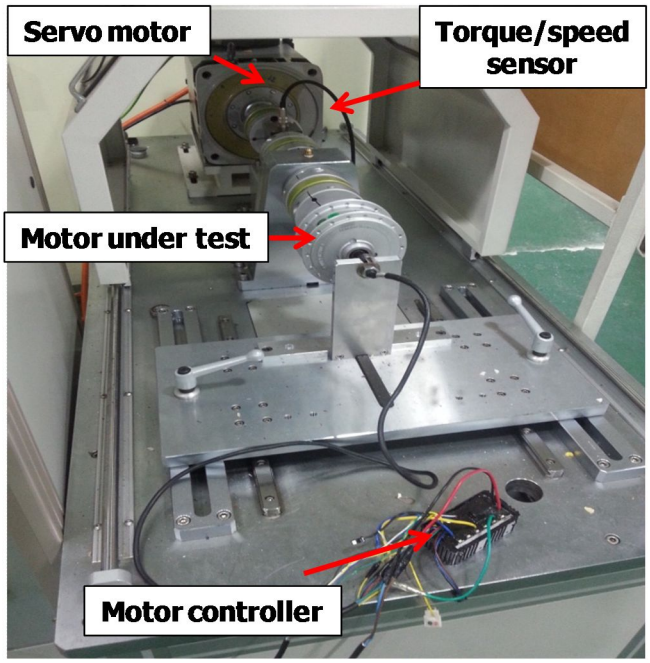

Fig 4.2 Picture of the dynamic simulator on motor dynamometer.

riding the e-bike, accelerating till 25 km/h and disengaging from power transmission. The time-speed profile acquired from the coastdown test was plotted in Fig 4.3. In order to find the running resistance corresponding to the reference speed, v_{ref} (6, 8, 10, 12, 14, 16, 18, 20 km/h), following equation (4.1) was applied.

$$T_{d,ref} = rF_{d,ref} = rm_a((v_{ref} + \Delta v)-(v_{ref} - \Delta v)) / \Delta t = 2\, rm_a \Delta v / \Delta t \qquad (4.1)$$

In equation (4.1), Δv is set as 2 km/h and Δt is the time interval elapsed until the e-bike's speed varies from $v_{ref} + \Delta v$ to $v_{ref} - \Delta v$ on the time-speed profile obtained from the coastdown test. The apparent mass, m_a, is the equivalent inertial mass including the total mass and the equivalent rotational inertia. In this study, the apparent mass was assumed to be the total mass multiplied by 1.03, which was reported in the previous research and the international standard.[3, 39] The running resistance torque calculated from equation (4.1) was fitted to the second order polynomial curve using the least square method and the resulting running resistance torque-speed correlation was expressed as the following equation (4.2) and shown in Fig 4.4

$$T_d = 2.3123 + 0.2576v + 0.00004v^2 \qquad (4.2)$$

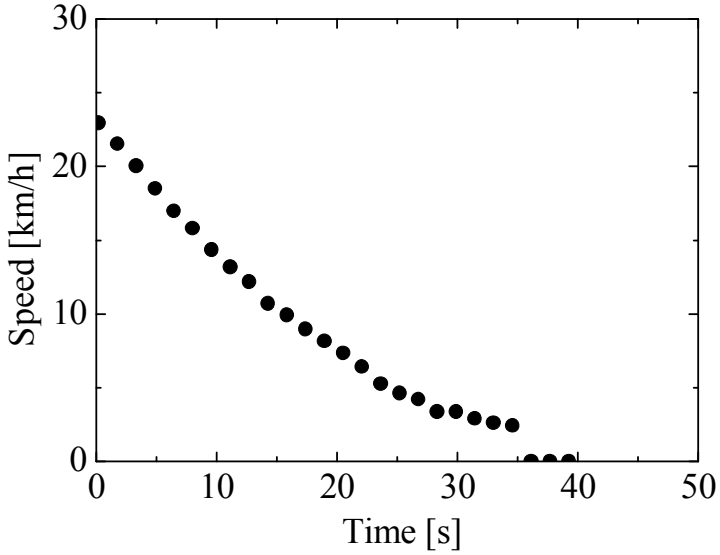

Fig 4.3 Time-speed profile of coastdown test on road

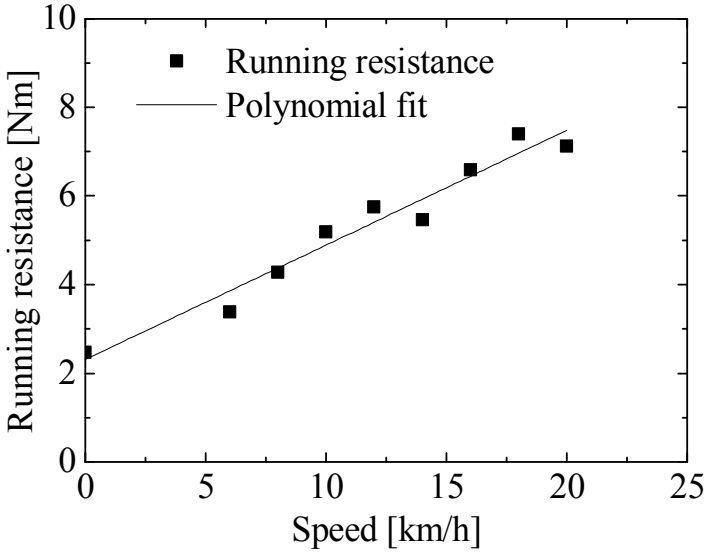

Fig 4.4 Running resistance torque-speed correlation on road

4.3.2 Acceleration test

We carried out the acceleration test in which we rode the e-bike by rotating fully and immediately the throttle in the handle to reach the maximum speed from the standstill. While acceleration test, we gathered the raw data including the rotating speed of the wheel, voltage and current of the battery. In acceleration test on the road, we accelerated the e-bike to reach the maximum speed for about 15 seconds from the start by rotating fully the throttle and after the e-bike reached the maximum speed, we released the throttle. Through the attained time-speed profile of the acceleration test, we ensured that the maximum speed of the test e-bike was about 23 km/h.

4.4 Dynamic simulation

4.4.1 Simulation process

The output torque of the in-wheel motor mounted on the center of the wheel was directly transferred to the surface of the road without the power loss of the transmission process through the differential gear, etc. So applying the equation (4.2), the e-bike's dynamic equation on the longitudinal way is expressed like the following equation (4.3).

$$T_m - T_d = T_m - (2.3123 + 0.2576v + 0.00004v^2) = J_a dw/dt = m_a r^2 dw/dt \qquad (4.3)$$

Equation (4.3) could be equally applied to the motor under test on motor dynamometer. Figure 4.5 shows the schematic diagram of dynamic simulation of motor dynamometer. A dynamic simulation is divided into the part controlling test motor speed and the part controlling the servo motor speed for implementing road load. A speed command to test motor is controlled by main control PC and is implemented in the form of analogue voltage through DAQ. A speed command to motor control unit (MCU) implements output signal of the e-bike throttle which operates in 1.2 ~ 3.5 V analogue voltage signal. In coastdown simulation, test motor runs at the maximum speed which is switched to coast drive when the power is cut off momentarily. In acceleration test, 3.5 V throttle output signal is sent to test motor MCU at standstill and the motor keeps running until reaching to the maximum speed.

During dynamic simulation, servo motor as a load machine is operated in speed control mode and thus continuous external speed command is needed. A speed command to servo motor is calculated using interaction equation among motor output, running resistance and motor rotation acceleration in equation (4.3). For obtaining a rotating speed of servo motor, a speed command should be given to servo motor while maintaining constant loop time responding to speed variation. In this study, a loop time for a speed command from a main control PC to servo motor was set as 200 ms and Figure 4.6 shows the loop

time occurred during acceleration test simulation, which was maintained constantly at 200 ~ 202 ms. Motor driver in servo motor has internal controller which controls a speed command received at 200 ms loop time as a set value. Internal controller controls servo motor speed using PI controller operating at approximately 1 ms interval. Figure 4.7 shows the dynamic simulation procedure in which the simulation is processed in the speed control mode of the servo motor as described in above. The program made on Labview acquired the data and controlled the above mentioned simulation logic and the block diagram of this program is shown in Fig 4.8.

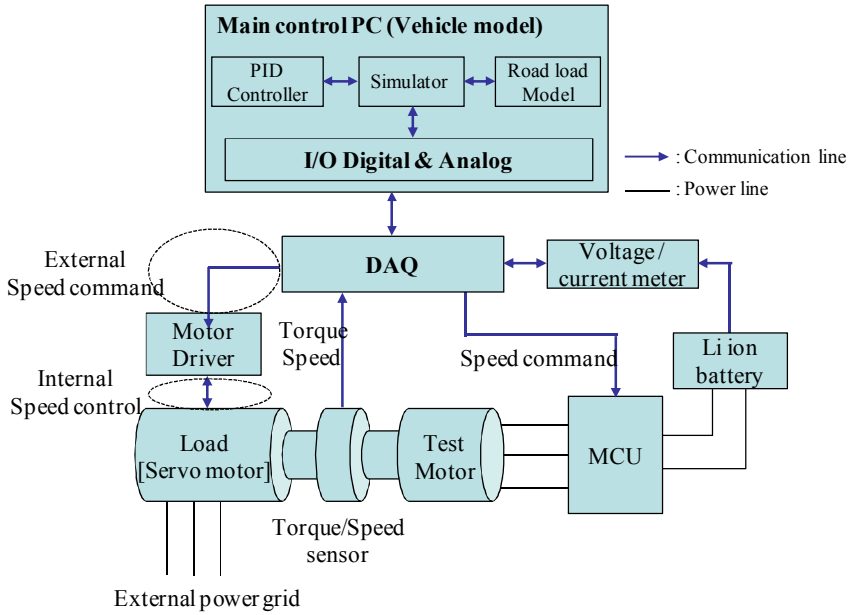

Fig 4.5 Schematic diagram of e-bike's dynamic simulation on motor dynamometer

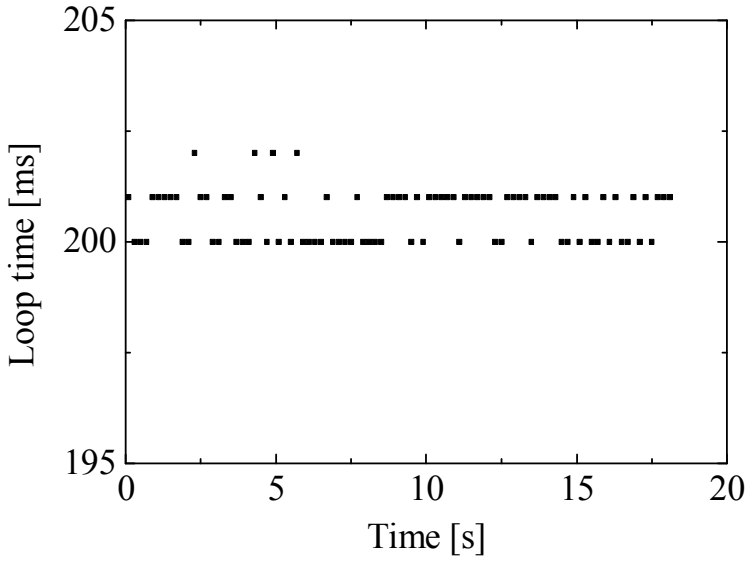

Fig 4.6 Loop time occurred during acceleration test simulation

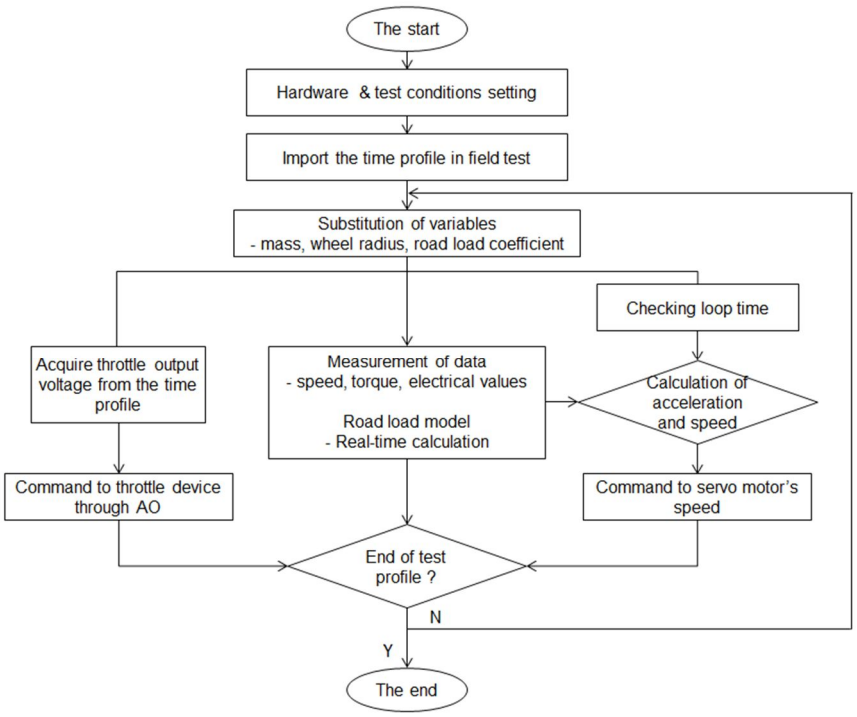

Fig 4.7 Dynamic simulation procedure with the servo motor operated at speed control mode

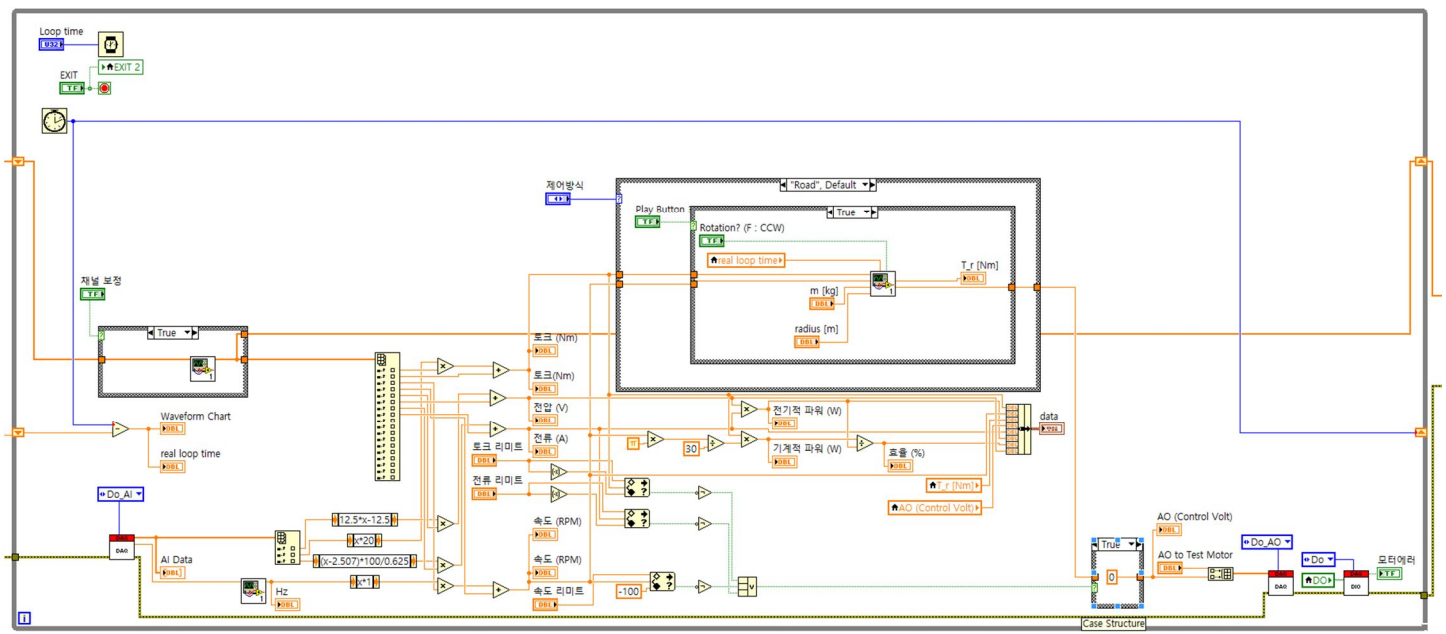

Fig 4.8 Block diagram of the control program made by Labview

4.4.2 Coastdown simulation

To evaluate the vehicle running performance in a chassis dynamometer, it's necessary to verify whether road load is appropriately set on chassis dynamometer. Such verification is implemented by comparing running resistances by reference speed which was obtained through coastdown data from chassis dynamometer and actual road test. [3] In a dynamic simulation developed in this study, road load factor in equation (4.2) from actual road test was set on a motor dynamometer, which was then followed by coastdown and compared with coastdown data from road test. Figure 4.9 shows the time-speed profiles obtained from the coastdown performed on road and motor dynamometer. As seen in Fig 4.9, dynamic simulator effectively simulated coastdown on road, and the travel distance during coastdown is calculated by integrating the speed by time and as a result, travel distance on actual road and motor dynamometer was 97.8 m and 98.5 m, respectively.

Figure 4.10 and Table 4.2 show the running resistances, at the reference speed, which were obtained from coastdown test on road and motor dynamometer. According to reference standard, tolerable error rate (ε, %) to running resistances on road and motor dynamometer was considered different according to the reference speed. Error rate, ε is defined by following

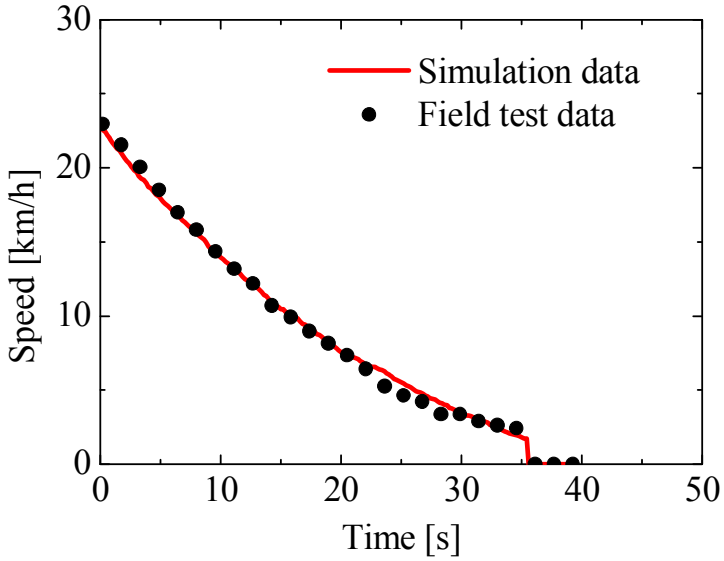

Fig 4.9 Time-speed profiles of coastdown tests on road and motor dynamometer

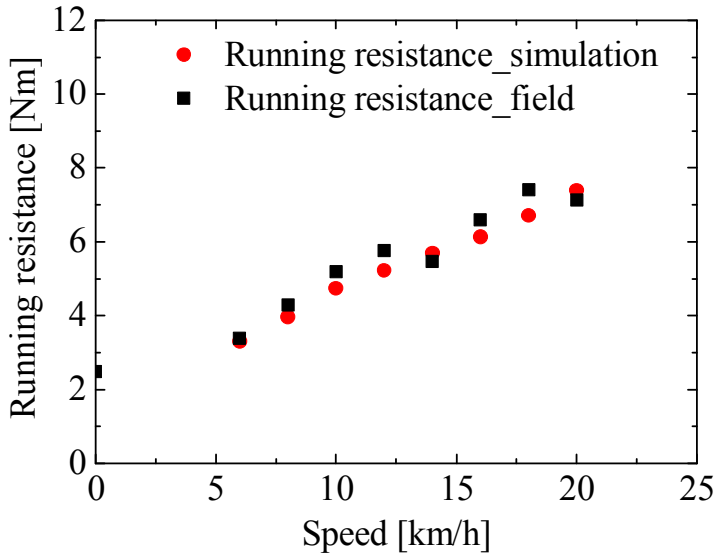

Fig 4.10 Running resistances by reference speed obtained from the coastdown test on road and motor dynamometer

Table 4.2 Running resistances according to reference speed on road and motor dynamometer.

Reference speed [km/h]	Running resistance [Nm]		Error rate, ε (%)
	Road	Motor dynamometer	
6	3.38	3.30	-2.37
8	4.28	3.97	-7.43
10	5.19	4.74	-8.66
12	5.76	5.22	-9.27
14	5.46	5.69	4.20
16	6.59	6.13	-6.99
18	7.40	6.71	-9.28
20	7.13	7.39	3.68

equation (4.4).

$$\varepsilon = (T_{d,r} - T_{d,m}) / T_{d,r}\ 100\ (\%) \qquad (4.4)$$

Especially, when reference speed was less than 30 km/h, error rate 10 % or less seemed to be acceptable as running resistance set at dynamometer. [3] As indicated in Table 4.2, error rate was 9.3 % in maximum and 2.4 % in minimum which were within 10 %, proving appropriate set at motor dynamometer.

4.4.3 Acceleration simulation

Figure 4.11, 4.12, and 4.13 show time-speed, time-voltage and time-current from acceleration test on road and motor dynamometer, respectively. As seen in Fig. 4.11, a dynamic simulation by motor dynamometer effectively simulated the e-bike's dynamic characteristics with the sudden speed increase accompanied by rotating fully and immediately the throttle in the handle. From the error analysis on time domain, we found out the maximum deviation of the speed in the simulation from the speed in the field test was ± 0.8 km/h and it can be assumed to be within the permissible error considering the measurement uncertainty of the measuring sensors such as the speed and

current sensors.

From the Fig 4.12 and 4.13, we could make sure the current to motor suddenly increased and the output voltage drop of the battery was followed at the moment of the starting from the standstill. These phenomena resulted from the sudden increase of the road load, especially inertial resistance at the moment of the starting from the standstill as seen in Fig 4.14. When it comes to the secondary battery including lithium ion battery and fuel cell, battery output voltage is decreased in line with increasing discharge current because of increase in such internal resistance as Ohmic loss. [44] Accordingly, the greater motor output is required and the battery output voltage is reduced because of increase in discharge current. As e-bike tested in this study has no such device as DC-DC converter which functions to maintain battery output at constant level, input voltage of motor controller varies depending on motor output. When motor input voltage varied, motor output rpm is accordingly varied because of the relationship between input voltage and back electromotive force. [55] Thus, to simulate the battery discharge characteristics as real as possible during actual road test and dynamic simulation, test condition was set to make battery OCV (open circuit voltage) and ambient temperature equal. [45, 46] As indicated in Fig 4.13, electric current through motor was 12.5 A in maximum which was attributed to motor

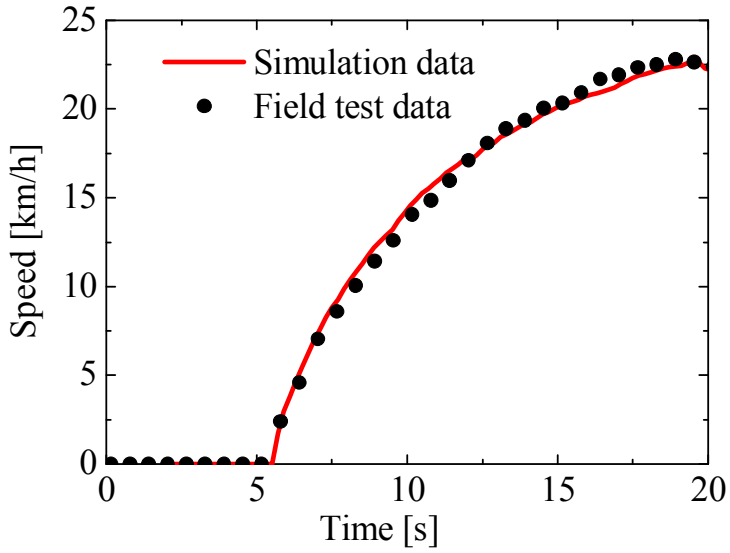

Fig 4.11 Time-speed relation from acceleration test on road and motor dynamometer

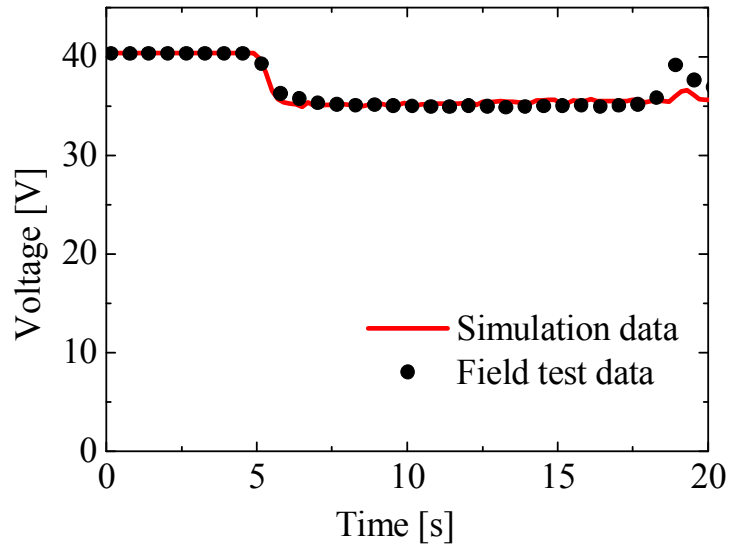

Fig 4.12 Time-voltage relation from acceleration test on road and motor dynamometer

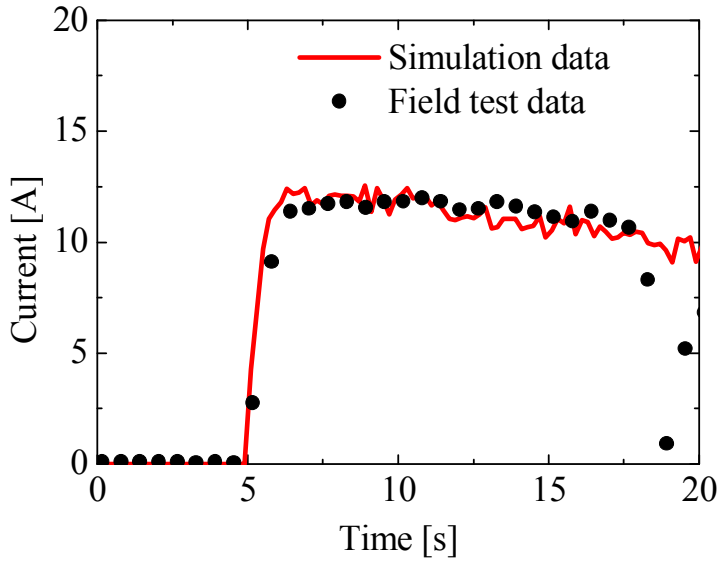

Fig 4.13 Time-current relation from acceleration test on road and motor dynamometer

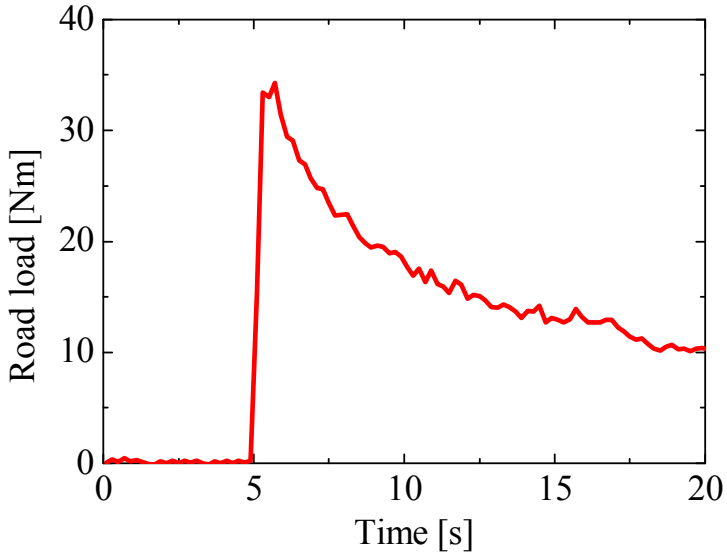

Fig 4.14 Time-road load profile in dynamic simulation during acceleration test

controller's overcurrent prevention function.

Figure 4.14 shows time-road load profile in dynamic simulation during acceleration test. Road load can be identified through the value measured by torque sensor on motor dynamometer which indicates the output torque of the drive motor. Inertial resistance is significantly increased at the moment when starting at standstill status, so that the maximum road load approaches approximately 34 Nm. In dynamic simulation, data including torque, speed, voltage and current were recorded at an interval of 200 ms and through recorded data, we could figure out the dynamic characteristics of the e-bike's drive motor at the moment of starting. As soon as the starting command from the throttle was delivered to MCU, torque, voltage and current simultaneously varied from the stop condition but the drive motor started to rotate 600 ms after the starting command. That is, the drive motor cannot rotate until the output torque reaches to 34 Nm and it means the drive motor needs at least additional time, 600 ms in order to overcome the road load at the moment of starting. Since reaching to maximum road load, an inertia resistance was gradually reduced and overall road load was also reduced over time. When the drive motor reached to maximum speed, about 23 km/h, the output torque of the drive motor was decreased to 10.1 Nm corresponding to one-third or less of the output torque at the start.

4.5 Energy efficiency evaluation on motor dynamometer

Energy efficiency of the electric two-wheeler was evaluated, analyzing the effect against the variation of the weight and the aerodynamic coefficient using the developed HILS on motor dynamometer. When the weight, m varied from 0.7m to 1.3m at intervals of 0.15m and the aerodynamic coefficient varied from $1.0C_2$ to $4.0C_2$ at intervals of $1.0C_2$, energy efficiency of the electric two-wheeler was evaluated and analyzed through the HIL simulation on motor dynamometer.

In general, if the weight of the vehicle including the riders increases, the energy efficiency becomes low. So the weight reduction of the vehicle is the one of the important design issues at the stage of the research and development of the vehicles. Because the weight reduction of the vehicle's parts without the reasonable trade-offs between the performance, cost, and safety may give rise to the unexpected problems involving the safety or reliability, the effect of weight has to be analyze thoroughly.

Evaluating the energy efficiency of the electric two-wheeler using the real one on road inevitably needs considerable times to test. But in this chapter, energy efficiency evaluation using HIL simulation on motor dynamometer needed just about 3 hours including the all cases about the variation of the weight and the aerodynamic coefficient.

4.5.1 Effect of the weight

If the vehicle's weight varies to some extents, the rolling resistances and the inertial resistances also are supposed to vary. So, the new road load models according to each weight have to be determined through the coast-down tests. But in this chapter, by references about relation between road load model and weight of vehicle, the coefficient about rolling resistances, C_0 and C_1, are assumed to be linearly proportional to the weight of vehicle. In field tests, the total weight of e-bike including the rider and the monitoring devices, m, was about 118 kg. In cases of 0.7m, 0.85m, 1.0m, 1.15m, 1.30m, the driving simulation through HILS on motor dynamometer was conducted.

Figure 4.15 shows the time-speed profiles in the cases of each weight. During the simulations on motor dynamometer, the test motor was rotated by the operator's manual control of the throttle device. As the increase of the weight, it was found the accelerating ability of e-bike when the accelerating intervals became worse. Figure 4.16 shows the plot about the relation between the weight of e-bike and the fuel efficiency. Comparing the 0.136 km/Wh of the energy efficiency in the case of 1.0m, the energy efficiencies in the case of 0.7m and 1.3m were 0.206 km/Wh and 0.095 km/Wh, respectively.

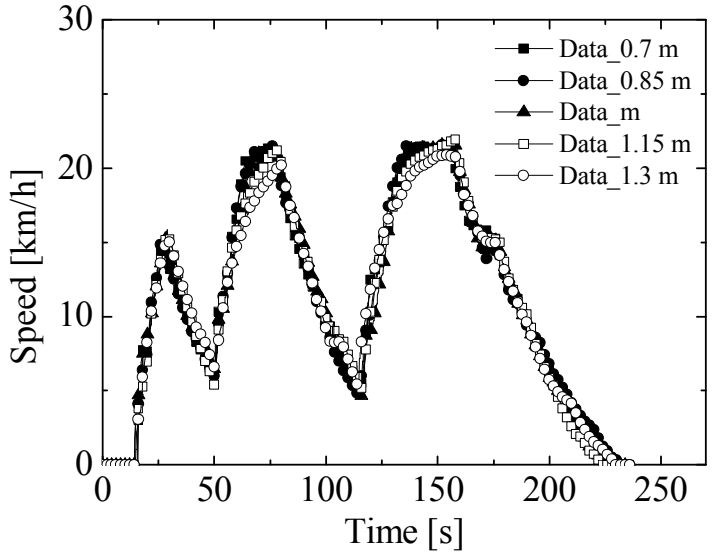

Fig 4.15 Time-speed profiles from HILS on motor dynamometer in the case of weight variation

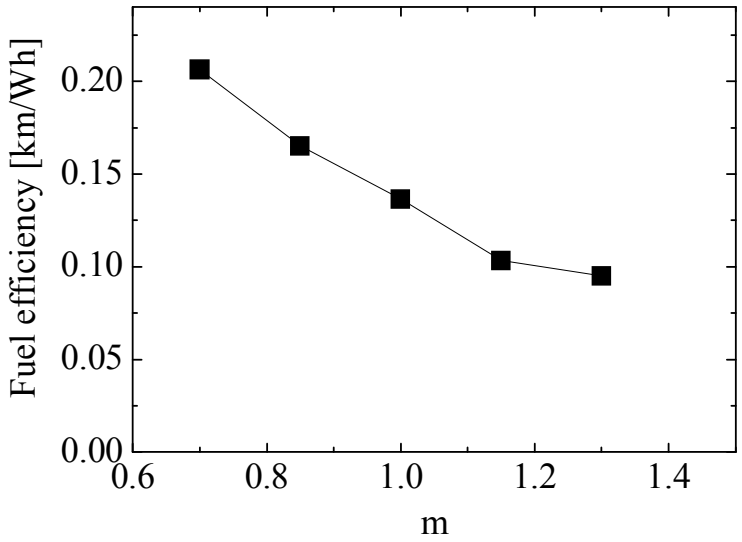

Fig 4.16 Relation between energy efficiency and weight

4.5.2 Effect of the aerodynamic resistance

The aerodynamic resistance of vehicle is mainly related with the outward appearance of vehicle subjected to the moving direction. In order to improve the energy efficiency of vehicle, the outward appearance is optimized so that the fluidic resistance is minimized. In this chapter, the aerodynamic resistance, C_2, was inserted differently into the road load model as C_2, $2C_2$, $3C_2$, $4C_2$.

Figure 4.17 shows the time-speed profiles in the cases of the each aerodynamic resistance. Unlike the time-speed profiles according to the weight variation described in previous chapter, the ones according to the aerodynamic resistance coefficients variation didn't have too much difference in each other. It was considered that the aerodynamic resistance had less effect in improvement of energy efficiency than the weight of vehicle in the case of the e-bike that run in relatively low speed. Figure 4.18 shows the plot about the relation between the energy efficiency and the aerodynamic resistance coefficient. When the aerodynamic resistance increased from C2 to 4C2, the energy efficiency of the e-bike decreased from 0.136 to 0.127 km/Wh.

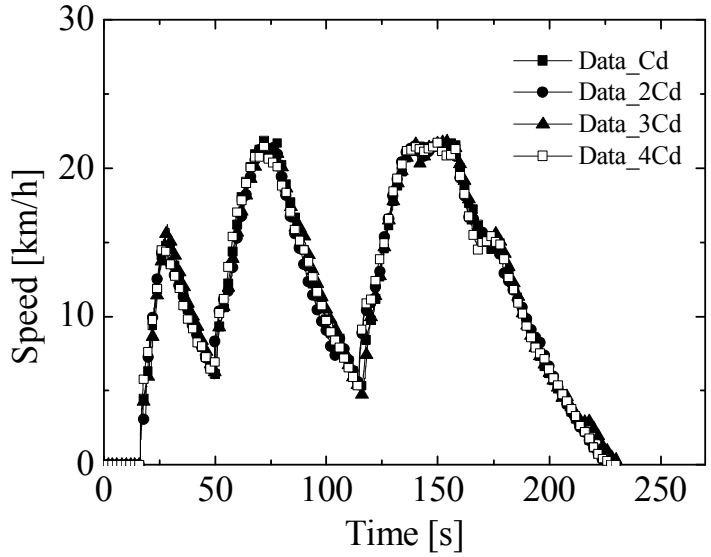

Fig 4.17 Time-speed profiles from HILS on motor dynamometer in the case of aerodynamic resistance variation

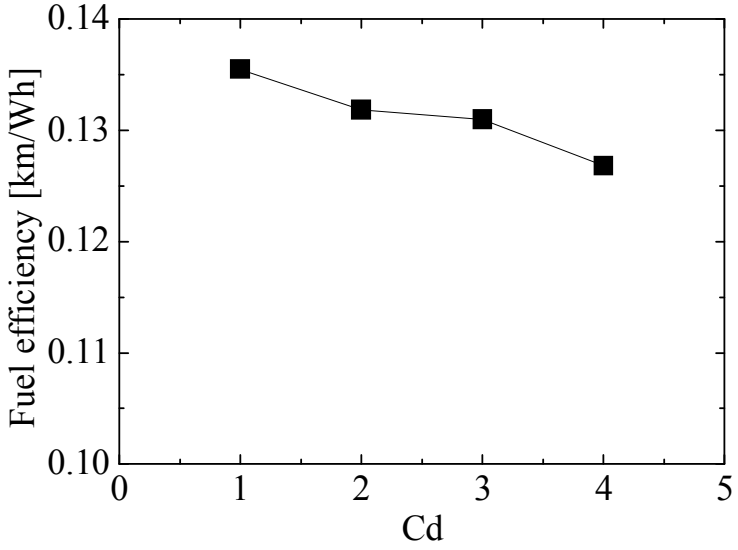

Fig 4.18 Relation between energy efficiency and aerodynamic resistance coefficient

4.6 Summary

Using a motor dynamometer equipped with servo motor, availability and feasibility of dynamic simulator which evaluate the running performance of e-bike were verified. Because the servo motor has the fast response to the operating command, we could precisely implement the dynamic drive characteristics of the e-bike at the condition of the acceleration and the coastdown during the simulation process on motor dynamometer. And by inserting the drive module including the motor, MCU, and battery into the simulation loop on the HIL test, the inrush current to motor and the battery voltage drop accordingly occurred at the moment of start was realized precisely.

As a result of comparing acceleration test and coastdown test on road, feasibility of dynamic simulation with motor dynamometer proved to be sufficient. In coastdown test where we drove about 100 m, the travel distance of the dynamic simulation had the deviation of 0.7 m from the travel distance on road test. And the error rate to running resistances on road and motor dynamometer was within 10 % to be acceptable at the reference speed. In acceleration test, the dynamic simulator simulated effectively the acceleration test on road as it had just 0.8 km/h error between the speed on road and motor dynamometer.

A dynamic simulator developed in this study is expected to be able to evaluate the performance and reliability of the motor, battery and controller under real condition without finished vehicle, and moreover, this dynamic simulator is also expected to be useful in evaluating (1) regenerative brake performance of electric motor, (2) fuel efficiency of motor-battery module and (3) studying on evaluation of motor-battery controller control algorithm.

Chapter 5. Conclusion

We developed a new method to determine the road load acting on an e-bike driven by in-wheel BLDC motor, different from the existing coastdown test. And this method was conducted by measuring the current consumption of the motor and using a correlation between the motor's torque and current when the e-bike is being driven at constant speed. Through the field test, we found that the e-bike motor's current consumption at constant speed could be used to derive the motor's output. After conducting field tests for five reference speeds, we obtained the second-order polynomial curve for speed and road load, from which the coefficients of rolling resistance, C_0, C_1, and the coefficient of aerodynamic resistance, C_D, were derived. The correlations between the speed and road load obtained from the new method and the coastdown were compared and analyzed. The maximum difference between the above two methods was 1.02 Nm and less than 1.0 Nm were in most sections of reference speeds. Considering a variety of measurement uncertainty factors, the error about less than 1 Nm suggests that the road load determined by the new method is highly reasonable. And the new method has the advantage that the road load can be acquired on a shorter driving track than possible in the coastdown test. For the new method, the driving track

should have a minimum length to allow the vehicle to cruise constantly at the maximum reference speed for more than 10 s. In the coastdown test, the e-bike was ridden for 97 m from 24 km/h to standstill. In contrast, in the new method, a driving track only about 60 m long was required for riding the e-bike and to cruise constantly at the maximum reference speed of 22 km/h for 10 s.

The new method was also verified through dynamic simulation on a motor dynamometer comprising the same real hardware as that mounted on the e-bike. When the e-bike's speed reached a rather constant value, we noticed that the motor was being subjected to the same road load as that when riding on a real road. Therefore, this method is expected to be used for determining the road load for e-bike whose the wheel drive electric motor is characterized by the linearity between torque and current. And we expect more extensive and detailed studies on this method will be conducted for various EVs, including e-bikes.

Next, the dynamic simulation, HILS at the mechanical level about the EV's drive motor was implemented on motor dynamometers equipped with the two load machines, the powder brake and the servo motor. Two types of dynamic simulation to evaluate the drive performance were conducted on two separate motor dynamometer equipped with the powder brake and the servo

motor. The real electric drive module consisting of the drive motor, MCU, and battery was inserted into the dynamic simulation loop and the road load generated by the powder brake and the servo motor was applied to these drive modules like the real driving condition on the road. While the powder brake generates a passive load locking the positive rotational move of the electric motor, the servo motor generates not only a passive load but also an active load such as accelerating positively the motor's rotation or coasting without the transmit of the power from the source like battery. On the motor dynamometer equipped with the powder brake, the dynamic simulation was conducted while the powder brake operated at the torque control mode. The drive performance of the e-bike such as the acceleration performance and the energy consumption efficiency was implemented on motor dynamometer using the powder brake. On the other hand, the servo motor implemented the coasting drive of e-bike on motor dynamometer in addition to the above mentioned driving simulation on motor dynamometer.

The dynamic simulator developed in this study is considered to be an effective means of pre-evaluation of drive motors or batteries prior to production of complete vehicles.

References

[1] ISO. Road vehicles-Road load-Part 1:Determination under reference atmospheric conditions. ISO 10521-1:2006.

[2] ISO. Road vehicles-Road load-Part 2:Reproduction on chassis dynamometer. ISO 10521-2:2006.

[3] ISO. Motorcycles-Methods for setting running resistance on a chassis dynamometer. ISO 11486:2006.

[4] ISO. Electric road vehicles - Reference energy consumption and range -- Test procedures for passenger cars and light commercial vehicles. 8714: 2002.

[5] ISO. Electric road vehicles -- Road operating characteristics. 8715: 2001.

[6] ISO. Battery-electric mopeds and motorcycles - Performance - Part 1: Reference energy consumption and range. 10364-1: 2012.

[7] ISO. Battery-electric mopeds and motorcycles -- Performance -- Part 2: Road operating characteristics. 2012: 2012.

[8] Jang GH, Yeom JH, Kim MG. Determination of torque-speed-current characteristics of a brushless DC motor by utilizing back-EMF of non-energized phase. Journal of Magnetism and Magnetic Materials. 2007;310:2790-2.

[9] Bouscayrol A. Different types of Hardware-In-the-Loop simulation for

electric drives. Industrial Electronics, 2008 ISIE 2008 IEEE International Symposium on: IEEE; 2008. p. 2146-51.

[10] Wagener A, Schulte T, Waeltermann P, Schuette H. Hardware-in-the-loop test systems for electric motors in advanced powertrain applications. SAE Technical Paper; 2007.

[11] Wu J, Dufour C, Sun L. Hardware-in-the-loop testing of hybrid vehicle motor drives at Ford Motor Company. Vehicle Power and Propulsion Conference (VPPC), 2010 IEEE: IEEE; 2010. p. 1-5.

[12] Ramaswamy D, McGee R, Sivashankar S, Deshpande A, Allen J, Rzemien K, et al. A case study in hardware-in-the-loop testing: Development of an ECU for a hybrid electric vehicle. SAE Technical Paper; 2004.

[13] Kim J, Jung D, Jeong C, Choi H. Worst-case scenario development based on Sine with Dwell test and evaluation for vehicle dynamics controller in UCC HILS. International Journal of Automotive Technology. 2014;15:961-6.

[14] Kwon J, Hong T, Park K, Heo S, Lee K, Kim W, et al. Robustness analysis of ESC ECU to characteristic variation of vehicle chassis components using HILS technique. International Journal of Automotive Technology. 2014;15:429-39.

[15] Yoon M-H, Lee J-m, Hong J-P. The Simulink Model of Motor System for HEV Using HILS (Hardware-In-the-Loop). Electromagnetic Field Problems

and Applications (ICEF), 2012 Sixth International Conference on: IEEE; 2012. p. 1-4.

[16] High-Performance Electric Motor Simulation Using the NI Electric Motor Simulation Toolkit. National instruments; 2014.

[17] Dufour C, Abourida S, Belanger J. Hardware-in-the-loop simulation of power drives with rt-lab. Power Electronics and Drives Systems, 2005 PEDS 2005 International Conference on: IEEE; 2005. p. 1646-51.

[18] He H, Xiong R, Zhao K, Liu Z. Energy management strategy research on a hybrid power system by hardware-in-loop experiments. Applied Energy. 2013;112:1311-7.

[19] Filipi Z, Fathy H, Hagena J, Knafl A, Ahlawat R, Liu J, et al. Engine-in-the-loop testing for evaluating hybrid propulsion concepts and transient emissions-HMMWV case study. SAE Technical Paper; 2006.

[20] Lin CF, Tseng CY, Tseng TW. A hardware-in-the-loop dynamics simulator for motorcycle rapid controller prototyping. Control Engineering Practice. 2006;14:1467-76.

[21] Oh SC. Evaluation of motor characteristics for hybrid electric vehicles using the hardware-in-the-loop concept. Vehicular Technology, IEEE Transactions on. 2005;54:817-24.

[22] Cherry CR, Weinert JX, Xinmiao Y. Comparative environmental impacts

of electric bikes in China. Transportation Research Part D-Transport and Environment. 2009;14:281-90.

[23] Dijk M, Orsato RJ, Kemp R. The emergence of an electric mobility trajectory. Energy Policy. 2013;52:135-45.

[24] Coelho MC, Luzia MB. Evaluating the energy performance of a SUV hybrid electric vehicle. Transportation Research Part D-Transport and Environment. 2010;15:443-50.

[25] Karner D, Francfort J. Hybrid and plug-in hybrid electric vehicle performance testing by the US department of energy advanced vehicle testing activity. Journal of Power Sources. 2007;174:69-75.

[26] Howey DA, Martinez-Botas RF, Cussons B, Lytton L. Comparative measurements of the energy consumption of 51 electric, hybrid and internal combustion engine vehicles. Transportation Research Part D-Transport and Environment. 2011;16:459-64.

[27] Cenek PD. Rolling Resistance Characteristics of New Zealand Road Surfaces. ASTM SPECIAL TECHNICAL PUBLICATION. 1994;1225:248-.

[28] Swift A. CALCULATION OF VEHICLE AERODYNAMIC DRAG COEFFICIENTS FROM VELOCITY FITTING OF COASTDOWN DATA. Journal of Wind Engineering and Industrial Aerodynamics. 1991;37:167-85.

[29] Morimitsu N, Nakagawa S. Development of simplified coastdown

method for road load calibration. SAE Technical Paper; 1984.

[30] Sakuma S, Sumi K, Mizutani Y, Matsushima S, Sugitani T. Development of High Performance Wheel Torque Measuring System and Its Applications. SAE Technical Paper; 1987.

[31] Passmore M, Jenkins E. A comparison of the coastdown and steady state torque methods of estimating vehicle drag forces. SAE Technical Paper; 1988.

[32] Berther T, Burkard H. Rotating Wheel Torque Meter with Telemetric Data Transmission. SAE Technical Paper; 2001.

[33] Páscoa JC, Brójo FP, Santos FC, Fael PO. An innovative experimental on-road testing method and its demonstration on a prototype vehicle. Journal of mechanical science and technology. 2012;26:1663-70.

[34] Bonhomme J, Mollón V. A Method to Determine the Rolling Resistance Coefficient by Means of Uniaxial Testing Machines. Experimental Techniques. 2013.

[35] Nabae A, Otsuka K, Uchino H, Kurosawa R. AN APPROACH TO FLUX CONTROL OF INDUCTION-MOTORS OPERATED WITH VARIABLE-FREQUENCY POWER-SUPPLY. Ieee Transactions on Industry Applications. 1980;16:342-50.

[36] Takahashi I, Noguchi T. A NEW QUICK-RESPONSE AND HIGH-EFFICIENCY CONTROL STRATEGY OF AN INDUCTION-MOTOR. Ieee

Transactions on Industry Applications. 1986;22:820-7.

[37] Guirong Z, Henghai Z, Houyu L. The Driving Control of Pure Electric Vehicle. Procedia Environmental Sciences. 2011;10:433-8.

[38] Tie SF, Tan CW. A review of energy sources and energy management system in electric vehicles. Renewable & Sustainable Energy Reviews. 2013;20:82-102.

[39] Preda I, Covaciu D, Ciolan G. Coast down test-Theoretical and experimental approach. 2010.

[40] Wu C, Tasi M, Mao S. Characteristics measurement of direct-drive brushless DC motors without using dynamometers. Electrical Machines and Systems, 2009 ICEMS 2009 International Conference on: IEEE; 2009. p. 1-6.

[41] IEEE. Guide Test Procedures for Direct-current Machines. ANSI/IEEE STD 113:1985.

[42] IEEE. Guide Test Procedure for Synchronous Machines. ANSI/IEEE STD 115:1983.

[43] IEEE. Standard Test Procedure for Polyphase Induction Motors and Generators. ANSI/IEEE STD 112:2004.

[44] Xiong R, He H, Guo H, Ding Y. Modeling for Lithium-Ion Battery used in Electric Vehicles. Procedia Engineering. 2011;15:2869-74.

[45] He HW, Xiong R, Guo HQ. Online estimation of model parameters and

state-of-charge of LiFePO(4) batteries in electric vehicles. Applied Energy. 2012;89:413-20.

[46] He HW, Zhang XW, Xiong R, Xu YL, Guo HQ. Online model-based estimation of state-of-charge and open-circuit voltage of lithium-ion batteries in electric vehicles. Energy. 2012;39:310-8.

[47] Lee S, Kim J, Lee J, Cho BH. State-of-charge and capacity estimation of lithium-ion battery using a new open-circuit voltage versus state-of-charge. Journal of Power Sources. 2008;185:1367-73.

[48] Ahlawat R, Jiang S, Medonza D, Smith MH. On emulating engine and vehicle transient loads for transmission-in-the-loop experiments. Mechatronics. 2012;22:989-96.

[49] Petersheim MD, Brennan SN. Scaling of hybrid-electric vehicle powertrain components for Hardware-in-the-loop simulation. Mechatronics. 2009;19:1078-90.

[50] Kim Y, Salvi A, Siegel JB, Filipi ZS, Stefanopoulou AG, Ersal T. Hardware-in-the-loop validation of a power management strategy for hybrid powertrains. Control Engineering Practice. 2014;29:277-86.

[51] Babbitt GR, Moskwa JJ. Implementation details and test results for a transient engine dynamometer and hardware in the loop vehicle model. Computer Aided Control System Design, 1999 Proceedings of the 1999 IEEE

International Symposium on: IEEE; 1999. p. 569-74.

[52] Fajri P, Ahmadi R, Ferdowsi M. Control approach based on equivalent vehicle rotational inertia suitable for motor-dynamometer test bench emulation of electric vehicles. Electric Machines & Drives Conference (IEMDC), 2013 IEEE International: IEEE; 2013. p. 1155-9.

[53] Zha H, Zong Z. Emulating Electric Vehicle's Mechanical Inertia Using an Electric Dynamometer. Measuring Technology and Mechatronics Automation (ICMTMA), 2010 International Conference on: IEEE; 2010. p. 100-3.

[54] Li Z, Deng Y, Xu P, Jin W, Xin J, Xiong X. Research of the hybrid power train dynamic test system. World Electr Veh J World Electric Vehicle Journal. 2011;4:635-41.

[55] Wildi To. Electrical machines, drives, and power systems. Upper Saddle River, N.J.: Pearson Education International; 2006.

국 문 초 록

본 연구에서는 전기이륜차의 도로부하를 측정하는 새로운 방법을 고안하고 모터 다이나모미터에서 주행성능을 평가할 수 있는 시뮬레이션 기법인 Hardware-in-the-loop simulation (HILS)에 대한 연구를 수행하였다. 차량의 성능을 평가하기 위한 방법에는 실도로 테스트와 샤시다이나모 테스트가 존재하지만, 주로 시험의 재현성 때문에 실험실 단위의 샤시다이나모 테스트가 이루어 지고 있다. 샤시다이나모 테스트를 위해서는 실도로에서 차량이 받는 도로부하를 정확히 측정하는 것이 매우 중요하며 타력주행(Coastdown)은 대표적인 도로부하 측정방법으로 활용되고 있다. 본 연구에서는 전기이륜차의 도로부하를 측정하기 위한 새로운 방법을 개발하였다. 도로 주행 시 차량이 등속으로 주행하게 되면 관성저항은 없기 때문에 엔진 혹은 구동 모터의 출력은 주행저항과 같게된다. 전기이륜차 구동모터의 출력토크는 소비전류와 선형 비례하며 이때 비례상수는 토크상수, k_t 로 표현된다. 등속 주행하는 전기이륜차의 모터 소비전류를 측정하고 이를 통해 모터의 출력토크를 계산하면 해당 속도에서의 주행저항을 산출할 수 있다. 구동 모터의 출력 토크와 소비전류와의 상관식은 모터 다이나모미터에서 특성시험을 수행하여 산출하였다. 또한 모터 특성시험과 실도로 시험 시에 모터 권선의

온도를 측정하여 모터의 열적 포화(Saturation)에 따른 모터 성능특성, 즉 출력 토크와 소비전류와의 영향을 분석하였다. 구동 모터가 열적 포화상태인 경우와 아닌 경우 각각 산출한 도로부하는 0.2 Nm 의 차이를 나타내었으며, 열적 포화상태가 아닌 경우와 타력주행에서 산출한 도로부하는 1.0 Nm 의 차이를 나타내었다. 본 연구에서 개발한 도로부하 측정 방법을 사용하면, 타력주행 시 회생제동 구현으로 타력주행 방법이 불가한 경우에도 도로부하 측정이 가능하며, 타력주행 대비 짧은 주행 도로에서도 도로부하 측정이 가능하다. 전기자전거를 실도로에서 주행하고 획득한 데이터를 근거로 하여 모터 다이나모미터에서 구동모터 시스템과 배터리에 실도로 주행환경을 모사하는 성능 시뮬레이션을 수행하였다. 주행 중 구동 모터가 받게되는 도로부하를 모터 다이나모 상에 동일하게 적용하기 위해서는 부하장치가 필요하며 본 연구에서는 파우더(Powder) 브레이크와 서보모터(servo motor)를 적용한 2 개의 테스트 베드에서 각각 동적 시뮬레이션을 수행하였다. 먼저 파우더 브레이크를 적용하여 구동 모터에 도로부하를 적용하였다. 속도에 따른 도로부하를 타력주행에서 얻은 속도-도로부하 상관식에서 계산하였으며, 이 값을 다시 PI 제어기의 설정값으로 제시하고 모터 다이나모에서 측정하는 현재값과 비교 보상함으로써 실시간으로 구동모터에 도로부하를

적용하였다. 파우더 브레이크는 수동부하 만을 줄 수 있기 때문에 속도제어는 불가능하며, 토크제어 모드에서 시뮬레이션은 수행되었다. 다음으로 서보모터를 이용하여 구동모터에 도로부하를 적용하였다. 서보모터는 속도제어 및 토크제어모드로 작동할 수 있기 때문에 파우더 브레이크와 달리 수동부하와 능동부하를 부여할 수 있다. 서보모터를 속도제어모드로 동작시켜 센서를 통해 측정된 토크값과 회전수 및 루프 경과시간을 계산하여 동적 시뮬레이션을 수행하였다. 본 연구에서 수행한 동적 시뮬레이션을 모터, 제어기, 배터리 등 구동 부품 평가에 적용할 경우, 실차 상태로 평가할 때 발생하게 되는 시간, 비용, 인력 등의 부담을 줄일 수 있을 것이다.

주요어: 전기이륜차, 도로부하, 토크상수, Hardware in the loop simulation (HILS), 모터 다이나모미터

학 번: 2009-31242